ELECTROSTATIC CHARGING IN FUEL FILTRATION

by

PETER WILLIAM HUBER

SUBMITTED IN PARTIAL FULFILLMENT

OF THE REQUIREMENTS FOR THE DEGREES OF

BACHELOR OF SCIENCE

AND

MASTER OF SCIENCE

IN MECHANICAL ENGINEERING

at the

MASSACHUSETTS INSTITUTE OF TECHNOLOGY

November, 1973

Signature of Author.....
Department of Mechanical Engineering

Certified by.....
Thesis Supervisor

Accepted by.....
Chairman, Department Committee on Graduate Students

ELECTROSTATIC CHARGING IN FUEL FILTRATION

by

PETER WILLIAM HUBER

Submitted to the Department of Mechanical Engineering on November 9, 1973, in partial fulfillment of the requirements for the degrees of Bachelor of Science and Master of Science in Mechanical Engineering.

ABSTRACT

A theory is presented for charge generation in fuel filtration. The charging process is modelled as an electrokinetic one resulting from fixed charge built up on the interior surfaces of the filter when in contact with a weak electrolyte such as fuel. Theoretical solutions for streaming currents and potentials developed in filtration are formulated for filters with uniform wall charges when the fluid Debye length is large compared with the mean radius of the filter pores. The functional dependence between streaming potentials and currents is obtained in terms of fluid properties, bulk filter characteristics, the fixed charge density and the tortuosity of the filter and flow conditions. The solutions are valid for filters thick compared with the fluid Debye length and for low flow rates when the filter is quasi-neutral as a whole. Charging experiments were carried out using Millipore filters through which n-heptane containing an ionizing additive was forced. Absolute comparisons between experimentally determined and theoretically predicted charging characteristics are shown to be very good.

Thesis Supervisor: Ain A. Sonin

Title: Associate Professor of Mechanical Engineering

Acknowledgements

This research was carried out with considerable help from many people to whom I am greatly indebted:

Dave Palmer and Dick Fenner gave valuable technical assistance in the experimental phases of the research.

Miss Eileen Gough typed the final copy of this thesis, enduring my handwriting and deciphering the illegible with manifest perseverance.

David Yung enlightened me on many of the finer points of membrane theory and laboratory politics.

Professor Sonin inspired and supervised the work throughout, providing constant encouragement, invaluable advice and inexhaustible patience without which this thesis would not have materialized.

This research was sponsored by the National Science Foundation under Grant No. GK-35798X.

Table of Contents

List of Appendicies

1. Charge relaxation for one-dimensional large Debye ratio flow.
2. Charge distribution across a diameter of a cylindrical pore.
3. The capillary model.
4. Effect of charge cloud on local conductivity.
5. The hydrocarbon fluid.
6. The ionizing additive.
7. Measurement of conductivity.
8. The Millipore filters.
9. Transient charging phenomena.
10. Comparison with hyperfiltration theory.
11. Flux equations in coupled form.

List of Figures

Nomenclature

a	pore radius (cm)
A	filter cross-sectional area (cm^2)
A	constant (dimensionless)
B	constant (dimensionless)
c	electrolyte concentration (mole cm^{-3})
c_i	concentration of ionic species i (mole cm^{-3})
c_u	concentration of undissociated electrolyte (mole cm^{-3})
c_o	cation concentration in neutral fluid (mole cm^{-3})
c_+	cation concentration (mole cm^{-3})
c_-	anion concentration (mole cm^{-3})
c_{+f}	fixed cation concentration (mole cm^{-3})
c_{-f}	fixed anion concentration (mole cm^{-3})
C	constant (dimensionless)
D	diffusion coefficient (cm^2 sec^{-1})
D_i	diffusion coefficient of ionic species i (cm^2 sec^{-1})
F	Faraday's constant (9.65×10^4 coulombs $mole^{-1}$)
h	filter thickness(cm)
I	net filter current (amp.)
I_m	net current in fluid (amp.)
I_s	net current in solid (amp.)
j	net current flux (amp. cm^{-2})
$\underline{j}$	net current flux in fluid (amp. cm^{-2})

j_i	current flux due to ionic species i (amp. cm^{-2})
j_s	net current flux in solid (amp. cm^{-2})
j_{fluid}	fluid flux rate (cm sec^{-1})
k	filter permeability (cm^{-2})
K	Kozeny constant (dimensionless)
ℓ	pore length (cm)
$\underline{\ell}$	coordinate of axial position (cm)
ℓ^*	pore length (dimensionless)
L_e	electrode spacing length (cm)
L_f	effective filter thickness (cm)
L_1	upstream electrode spacing (cm)
L_2	downstream electrode spacing (cm)
L_{11}, L_{12}, L_{21}, L_{22}	Onsager coefficients
n	number of pores in a filter (dimensionless)
P	pressure (dyne cm^{-2})
Pe	Peclet number (dimensionless)
Q	superficial flow rate (cm^3 sec^{-1}),
r	coordinate of radial position (cm)
r^*	coordinate of radial position (dimensionless)
R	gas constant (8.31 x 10^{-1} erg gm-mole^{-1} $^oK^{-1}$)
R_e	effective electrode resistance (ohms)
R_f	effective filter resistance (ohms)

S_o	specific filter surface exposed to fluid (cm^{-1})
T	temperature (^oK)
T	filter tortuosity (dimensionless)
$\underline{v}$	flow velocity ($cm\ sec^{-1}$)
V	mean flow velocity ($cm\ sec^{-1}$)
x	coordinate of axial position (cm)
x^*	coordinate of axial position (dimensionless)
z	charge number (dimensionless)
z_i	charge number of ionic species i (dimensionless)
α	constant
δ_D	effective sheath thickness (cm)
ΔP	pressure drop ($dyne\ cm^{-2}$)
$\Delta\phi$	potential drop (volts)
$\Delta\phi_{el\ e2}$	potential drop across electrodes (volts)
$\Delta\phi_{12}$	potential drop across filter (volts)
$\Delta\phi_{I\ II}$	potential drop across filter (volts)
ε	filter porosity (dimensionless)
ε_r	relative permitivity (dimensionless)
ε_o	permitivity of free space (8.85×10^{-14} sec $ohm^{-1}\ cm^{-1}$)
λ_D	Debye length (cm) ($\lambda_D = \left(\varepsilon \frac{\varepsilon_r D}{\sigma_m}\right)^{1/2}$)
λ_D^*	Debye ratio (dimensionless)
μ	fluid viscosity ($dyne\ sec\ cm^{-2}$)
ξ	coordinate of axial position (cm)
ξ^*	coordinate of axial position (dimensionless)
ρ	charge density ($coulombs\ cm^{-3}$)

ρ_f fixed charge density (coulombs cm^{-3})

$\bar{\rho}_f$ mean fixed charge density (coulombs cm^{-3})

ρ_m mobile charge density (coulombs cm^{-3})

$\bar{\rho}_m$ mean mobile charge density (coulombs cm^{-3})

ρ_o absolute charge in neutral fluid (coulombs cm^{-3})

ρ^* charge ratio (dimensionless)

σ conductivity (ohm^{-1} cm^{-1})

σ_f effective filter conductivity (ohm^{-1} cm^{-1})

σ_m fluid conductivity (ohm^{-1} cm^{-1})

σ_s solid conductivity (ohm^{-1} cm^{-1})

σ_o neutral fluid conductivity (ohm^{-1} cm^{-1})

ϕ electric potential (volts)

ϕ_o filter streaming potential (volts)

ϕ^* electric potential (dimensionless)

ϕ_w^* wall potential (dimensionless)

1. Introduction

Charge generation and transport during the flow of hydrocarbon liquids past surfaces is a problem of practical importance in the handling of gasolines and other fuels. Sufficient electrostatic charges can be generated in pipe flow and filtration to produce spontaneous electrical discharges in the ambient atmosphere, resulting in ignitions and explosions[1]. Filtration is a particularly important aspect of this charging problem because of the large solid-fluid interfaces involved. Consequently an analysis of charging characteristics for flow through filters establishing the dependence of charging currents and potentials on fluid and filter properties and flow parameters is essential in evaluating hazards in fuel handling operations.

The physical mechanism of charge generation in flows past surfaces is qualitatively well understood. A fixed charge is acquired by the solid surface, by ion adsorption from the fluid, for example. Overall charge neutrality is maintained by the presence of an equal amount of mobile charge of the opposite sign which exists in the fluid near the solid-fluid interface.A charge "double-layer" (the Gouy-Chapman double-layer or Debye sheath) is thus formed, extending a characteristic distance of one Debye length into the fluid[2]. If the fluid is caused to flow adjacent to the solid surface by means of an applied pressure the mobile charge in the fluid will be convected with it, giving rise to streaming currents and potentials.

A number of investigators have studied charging porblems in filtration on an empirical basis[3]-[6] but no adequate theoretical

treatment of the problem has yet been presented. Theoretical studies of related problems using the techniques of irreversible thermodynamics have been carried out[7], but while these are revealing in many ways, they do not assign a physical significance to the Onsager coefficients, nor do they provide insight into the mechanisms actually involved in charge generation. The present work proposes a relatively simple physical model for the electrostatic structure and flow geometry of a filter and derives expressions for charging currents in fuel filtration for a range of flow parameters. The analysis makes use of an important simplification of the problem which is valid for most cases of hydrocarbon filtration. The double layers formed for low conductivity liquids such as fuels will usually extend macroscopic distances into the fluid - a phenomenon rarely encountered with higher conductivity aqueous solutions. When the fluid Debye length is large compared with the mean pore radius of a filter through which the fluid is passed, but small compared with the filter thickness, an analysis of the concomitant charging problems can be formulated quite simply. In this study large Debye lengths are assumed in our model, which we use to derive functional relationships between streaming currents, potentials, flow parameters and filter characteristics for some simple flow conditions. Also included are experimental results which verify the validity of our model, at least for the range of parameters tested. While the present solution lacks generality in that it places an upper bound on the flow velocities permitted, the experimental results indicate that our model is extremely promising and has yet to be fully exploited.

2. Theory

2.1 Model

The model we have adopted for the electrostatic structure of a filter is based on the assumption, common in explaining electrokinetic pheonomena, that the solid parts of a filter acquire a fixed charge as a result of ion adsorption, surface chemical reactions or other processes[8]-[10]. The fixed charge may be distributed either on the interior surfaces of the filter or within its solid matrix. Balancing the fixed charge is an equal amount of mobile charge of the opposite sign which exists as a charge cloud within the interstices of the filter and to some extent outside it.

The exact distribution of the charge cloud in space for a uniform fixed charge distribution in the filter will depend on the flow conditions and fluid properties (Appendix 1). The governing parameter is the Peclet number based on Debye length, Pe , defined by:

$$Pe \equiv \frac{V\lambda_D}{D} \tag{1}$$

where V is the mean flow velocity within the filter, λ_D the fluid Debye length and D the diffusion coefficient of the ions in the fluid. We note here that when the Peclet number is small compared with unity a filter which is thick compared with the Debye length may be considered to be quasi-neutral as a whole. In this case virtually all mobile charge resides inside the filter, rather than outside it,in charge clouds. This means that the fixed charge within the filter and the mobile charge in the filter interstices must approximately balance at all points inside the

filter. If we express the mean fixed charge density $\bar{\rho}_f$ contained in the filter as a fixed charge per unit void volume then this must equal in magnitude the mean mobile charge density $\bar{\rho}_m$ in the void regions of the filter (Fig. (1)). The quasi-neutrality equation for points within the filter can then be written as:

$$\bar{\rho}_f + \bar{\rho}_m = 0 \qquad (2)$$

While fixed charge cannot, by definition, exist in the filter interstices it is in these regions that electrostatic effects are manifested, and we will, as a matter of convention, express fixed charge densities per unit void volume of the filter. In the present work we will restrict Peclet numbers to values small compared with unity and thus make this simple statement of quasi-neutrality, although neither step is essential to the model.

We next consider the large Debye ratio assumption which will also be made throughout this analysis. The mobile charge distribution across a diameter of a cylindrical pore bearing a fixed surface charge can be shown to be a function of the Debye ratio λ_D^* - the Debye length λ_D of the fluid contained in the pore divided by the pore radius a - when the pore length is large compared with the Debye length. The Debye length of a fluid is given by $\lambda_D = \sqrt{\varepsilon_r \varepsilon_o D/\sigma}$ where ε_r is the relative permitivity of the fluid, ε_o the permitivity of free space and σ the local conductivity of the fluid (Eq. (A2.2), Appendix 2). Fig. (2) shows the variation of mobile charge density ρ_m for varying Debye ratios as a function of radial position r. These curves are based on a linearized from of the charge distribution equation assuming a low wall charge (Appendix 2). The important limit, for the purposes of our model, is when the Debye ratio is large compared with unity. In this case, as shown in Fig. (2), ionic concentration gradients across a pore diameter disappear. While this

result is easily derived only for a simple pore geometry and for low wall charges, it is clear that it will be generally valid even for complex pore geometries and high wall charges provided the Debye ratio is sufficiently large. Thus for flow through a filter, ionic concentration gradients in any direction perpendicular to a solid surface within the filter may be considered negligible provided the Debye ratio based on the mean filter pore radius is large. Extremely low conductivities are commonly encountered in hydrocarbon fluids, giving rise to relatively large Debye lengths and justifying the analysis of charging problems for large Debye ratio filtration. A gasoline of conductivity $10^{-14}\ \Omega^{-1}\ cm^{-1}$, for example, will have a Debye length of about .02 cm, this to be compared with aqueous solutions where the Debye length is typically measured in Angstroms.

In the present analysis we will thus model the electrostatic structure of a filter and the flow conditions through it with the following assumptions:

(a) The fixed charge is uniformly distributed on the solid surfaces or within the solid matrix of the filter.

(b) The Debye ratio based on mean filter pore radius is large compared with unity.

(c) The filter thickness is large compared with the fluid Debye length.

(d) The Peclet number based on Debye length for flow through the filter is small compared with unity.

If these four conditions are met the mobile charge cloud in a filter will be uniformly distributed throughout the interstitial regions of the filter Furthermore the mean mobile charge density in the void regions of the filter will equal in magnitude the fixed charge density (expressed per unit void volume of filter) existing within the filter (Eq. (2)). This model for the electrostatic structure of a filter is schematically shown in Fig. (3).

Before proceeding to solve the ionic flux equations through a filter on the basis of this model we consider definitions of path length through a filter and mean flow velocity within a filter consistent with bulk filter properties and behavior. The architecture of a real filter, membrane or porous bed is complex and to a large extent random. We can, however, define the ratio of the effective distance travelled by a typical fluid particle in moving through a filter to the filter thickness as the tortuosity T, a physical property of the filter.* The tortuosity of a filter can be related by means of a simple capillary model which assumes Poiseuille flow within the filter to the Kozeny constant K (Appendix 3) by:

$$T = \frac{1}{\sqrt{2K}} \tag{3}$$

The Kozeny constant has a value of .2 for a wide class of porous materials[11] indicating typical filter tortuosities of about 1.6. The capillary model also gives an expression for the mean flow velocity V within the filter in terms of the superficial flow rate through the filter Q, the filter tortuosity T, porosity ε and cross-sectional area A (Appendix 3):

$$V = \frac{QT}{\varepsilon A} \tag{4}$$

With these expressions for effective path length through a filter and

---

* This definition of tortuosity differs from that adopted by some other investigators who define tortuosity as a ratio of hypothetical to actual filter permeabilities (Appendix 3).

mean flow velocity within a filter together with the electrostatic model described we shall solve for ion fluxes through a filter and hence obtain expressions for streaming currents and potentials developed in steady flows.

2.2. Equations, Parameters and Solutions

Ion fluxes in a fluid medium may result from three driving mechanisms: convection in a flow field, diffusion along a concentration gradient and migration in an electric field. In this analysis we assume these effects are uncoupled - a good approximation for the dilute solutions formed in most hydrocarbon liquids. The Nernst-Planck flux equation for the current flux $\underline{j}_i$ due to a single dilute ionic species i is :

$$\underline{j}_i = Fz_i c_i \underline{v} - Fz_i D_i \nabla c_i - \frac{F^2 z_i^2 D_i c_i}{RT} \nabla\phi \tag{5}$$

Here F is Faraday's constant, z_i the charge number, c_i the local ion concentration, $\underline{v}$ the flow velocity, D_i the diffusion coefficient R the gas constant, T the temperature and ϕ the electric potential. To obtain the overall current flux $\underline{j}$, Eq. (5) is summed over all ionic species, and substitutions for the local mobile charge density ρ_m in a fluid and for σ, the local fluid conductivity are made using Eq. (6) and Eq. (7):

$$\rho_m = \sum_i Fz_i c_i \tag{6}$$

$$\sigma = \sum_i \frac{F^2 z_i^2 D_i c_i}{RT} \tag{7}$$

$$\underline{j} = \underline{v}\,\rho_m - \nabla \left(\sum_i Fz_i D_i c_i\right) - \sigma \nabla\phi \tag{8}$$

Next we impose the boundary conditions required by our electrostatic model for a filter on Eq. (8). If all ions have approximately equal diffusion coefficients, diffusive effects within the filter disappear as

a result of the uniformity of the mobile charge density within the filter, and the flux equation becomes:

$$\underline{j} = -\underline{v}\ \bar{\rho}_f - \sigma\nabla\phi \tag{9}$$

In Eq. (9) the mobile charge density within the filter has been replaced by the negative of the mean fixed charge density in the filter. This step is justified by the quasi-neutrality assumption (Eq. (2)) together with the fact that the mobile charge density ρ_m will equal the mean value $\bar{\rho}_m$ at all points in the filter intertices when the Debye ratio is large.

We may integrate the flux equation along a particle path from a point within the filter on the upstream edge to a point within the filter on the downstream edge and therby obtain a characteristic integrated flux equation for points in the void regions of the filter. The integration to be performed is shown schematically in Fig.(4). In our model the mean fixed charge density is taken to be uniform along such a path and the fluid conductivity inside the filter σ_m, is therefore constant (although not necessarily equal to the fluid conductivity at points outside the filter). The integration may be represented as:

$$\int_1^2 \underline{j} \cdot d\underline{\ell} = -\bar{\rho}_f \int_1^2 \underline{v} \cdot d\underline{\ell} - \sigma_m \int_1^2 d\phi \tag{10}$$

The convective term of Eq. (10) is replaced by the product of the mean flow velocity V within the filter (Eq. (4)) and the path length of the integration which is defined as the product of the filter tortuosity T and the filter thickness h. The net potential drop from point 2 to point 1 is designated $\Delta\phi_{12}$ and is obtained from the integrated flux

equation as:

$$\Delta\phi_{12} = -\frac{QT\,\bar{\rho}_f\,Th}{\varepsilon A\sigma_m} - \frac{jTh}{\sigma_m} \qquad (11)$$

Eq. (11) relates the mean current flux j in the filter interstices to the mean potential drop across the filter for points within the filter. To convert these to actual potentials and currents developed outside the filter we must consider changes that occur over the inlet and outlet regions of the filter. Current continuity requires that at steady state the net current flux outside the filter be equal to the product of the net current flux within the filter and an area ratio which is the total pore cross-sectional area divided by the filter cross-sectional area. Changes in potentials across the inlet and outlet are not as easily obtained. Direct application of the complete flux equation is difficult because quasi-neutrality does not apply over the inlet or outlet (Fig.(1)). Furthermore, substantial changes in fluid conductivity may occur in these regions. An order of magnitude analysis of the terms in Eq. (8) reveals, however, that when convective fluxes dominate diffusive fluxes over distances of the order of the filter thickness (as is the case in the model we have adopted) then over distances small compared with the filter thickness fluxes due to diffusion and electric migration must approximately balance. This means that over distances small compared with the filter thickness a Boltzmann quasi-equilibrium must exist. For the low Peclet number flows which we are considering inlet and outlet effects occur over a characteristic distance of one Debye length (Appendix 1, Fig.(1)), a distance we take to be small compared with the filter thickness. Thus over the inlet and outlet regions of the filter a Boltzmann quasi-equilibrium must be established and potential changes must be functions of concentration

ratios only. If the permeating fluid is a weak electrolyte, as are most hydrocarbon liquids, the ionic concentrations in the relaxed (neutral) fluid will be identical upstream and downstream of the filter as long as temperatures are equal. This means that the potential difference across the inlet must be exactly equal in magnitude and opposite in sign to the potential difference across the outlet of the filter since ion concentrations in the filter are uniform throughout the filter. We can then write Eq. (11) in terms of the current I_m in the bulk of the fluid and the potential difference between points I and II immediately upstream and downstream of the filter (Fig.(4)):

$$\Delta\phi_{I\ II} = -\frac{QT\ \bar{\rho}_f Th}{A\varepsilon\sigma_m} - \frac{I_m Th}{A\varepsilon\sigma_m} \tag{12}$$

This equation does not include the possibility of current "leakage" by conduction through the solid parts of the filter. If the solid constituent has conductivity σ_s then the current flux $\underline{j}_s$ within the solid matrix is determined by Ohm's law:

$$\underline{j}_s = -\sigma_s \nabla\phi \tag{13}$$

Integrating this and substituting for the current I_s through the solid and for the effective solid cross-sectional area we obtain:

$$I_s = -\frac{\sigma_s A(1-\varepsilon)}{Th}\ \Delta\phi_{I\ II} \tag{14}$$

The net current flowing through the filter is the sum of the current through the solid parts as predicted by Eq. (14) and the current through the fluid specified in Eq. (12). Thus we can write:

$$\Delta\phi_{I\ II} = -\frac{QT\ \bar{\rho}_f\ Th}{A\varepsilon\left(\sigma_m + (\frac{1-\varepsilon}{\varepsilon})\sigma_s\right)} - \frac{I\ Th}{A\varepsilon\left(\sigma_m + (\frac{1-\varepsilon}{\varepsilon})\sigma_s\right)} \tag{15}$$

where I is the net current through the filter. Eq. (15) can be written in the form:

$$\Delta\phi_{I\ II} = \phi_o - IR_f \tag{16}$$

$$\phi_o = -\frac{V\,\bar{\rho}_f \varepsilon L_f}{\sigma_f} \tag{17}$$

$$R_f = \frac{L_f}{A\sigma_f} \tag{18}$$

$$L_f = Th \tag{19}$$

$$V = \frac{QT}{\varepsilon A} \tag{4}$$

$$\sigma_f = \varepsilon\sigma_m + (1 - \varepsilon)\sigma_s \tag{20}$$

For a weak binary electrolyte the conductivity σ_m of the fluid within the filter can be related to the fixed charge density in the filter and the bulk fluid conductivity σ_o, (Appendix 4) by:

$$\frac{\sigma_m}{\sigma_o} = \rho^* + \frac{1}{\rho^* + \sqrt{\rho^{*2} + 1}} \tag{21}$$

$$\simeq \rho^* \quad \text{when} \quad \rho^* >> 1 \tag{22}$$

$$\simeq 1 \quad \text{when} \quad \rho^* << 1 \tag{23}$$

Here $\rho^* = |\bar{\rho}_f/\rho_o|$ and ρ_o is the absolute charge in the bulk, neutral fluid computed by assuming all ions to be of the same sign:

$$\rho_o \equiv \frac{\sigma_o RT}{zFD} \tag{24}$$

Thus a further parameter of the charging problem is the charge ratio ρ^*, defined as the ratio of the fixed charge density in the filter to the absolute charge of the bulk fluid. For low charge ratios ($\rho^* << 1$) the conductivity of the fluid within the filter is essentially equal to the conductivity σ_o of the bulk fluid, and the expression for σ_f (Eq. 20) is of the form:

$$\sigma_f \approx \varepsilon\sigma_o + (1-\varepsilon)\sigma_s \tag{25}$$

For high charge ratios ($\rho^* >> 1$) the conductivity of the fluid within the filter differs substantially from that of the bulk fluid. In this case the expression for σ_f is modified:

$$\sigma_f \approx \varepsilon\sigma_o\rho^* + (1-\varepsilon)\sigma_s \tag{26}$$

and the expression for ϕ_o (Eq. 17) can be written:

$$\phi_o \approx \frac{RT}{zF} \frac{VL_f}{D + \left(\frac{1-\varepsilon}{\varepsilon}\right)\left(\frac{\sigma_s RT}{zF\rho^*}\right)} \tag{27}$$

Eq. (16) gives the functional relationship between potential across the filter and the filter current but does not take into account the Ohmic resistance of the fluid between the measuring electrodes upstream and downstream of the filter. In general the measuring electrodes are not immediately adjacent to the filter and this resistance, which depends on

the precise geometry of the fluid regions separating the filter and the electrodes, must be considered. For the case of one-dimensional flow with two electrodes at distances L_1 and L_2 from a filter (Fig. (5)), such that the total length of fluid between the electrodes and the filter is L_e, the potential developed between the electrodes, $\Delta\phi_{e1\ e2}$ is obtained from Eq. (18) by replacing R_f with:

$$R_f + R_e = \frac{L_f}{A\sigma_f} + \frac{L_e}{A\sigma_o} \tag{28}$$

The solution stated in Eq. (16) - Eq. (28), the range of parameters for which they are valid and the properties on which they depend are summarized in Table 1 and Fig. (5).

3. Experiments

A series of experiments was conducted to test the validity of the solutions derived in Section 2. Previous experimental investigations of related charging problems[3]-[6] have been largely for flow conditions not considered in the present theory. In our experiments with filters of precisely known characteristics we were able to ensure that high Debye ratios and low Peclet number flows were attained.

The hydrocarbon fluid used in our charging experiments was n-heptane, a short chain aliphatic compound, typical in many ways of a wide class of organic fluids (Appendix 5). The conductivity of the heptane was varied using an antistatic additive, Shell ASA #3, kindly provided by Shell Chemical Company (Appendix 6). ASA #3 is manufactured specifically for the purpose of increasing conductivities of fuels and thereby reducing charging hazards in fuel handling operations. Conductivity measurements were made immediately after each charging experiment using a direct current method commonly adopted for petroleum products (Appendix 7). Cellulose ester filters manufactured by Millipore Company (Appendix 8) were chosen for the tests, primarily because they are available in controlled thicknesses, pore sizes and chemical composition and purity. Millipore filters and chemically similar collodion (cellulose nitrate) membranes have been studied in related membrane experiments[8],[9] and some previous information about the electrical structure of these filters is therefore available.

3.1 Charge generation apparatus

The charge generation apparatus was designed to measure streaming currents and potentials for one dimensional flow through one or more Millipore filters in intimate contact with each other. The apparatus consisted of two stainless steel tanks for storing and collecting the heptane and a test cell (Fig. (6)) in which the filter and measuring electrodes were mounted. One tank was pressurized with oil-free nitrogen causing the heptane to flow into the upstream side of the test cell. The heptane passed through the filter and was collected from the downstream side of the cell in the second tank.

The test cell was made of Plexiglass, and "Poly-flo" (polyethylene) tubing was used for all connections. Viton O-ring seals separated the two sides of the filter from each other. Movable stainless steel mesh electrodes on each side of the filter were used to measure streaming potentials and currents. It was clearly impractical to attempt to obtain streaming potentials and currents with electrode spacings small in comparison with filter thicknesses, which were of the order of .01 cm. All data obtained was therefore with about 100 filter thicknesses or more separating the electrodes from the filter. All metal parts upstream of the filter, including the upstream electrode were connected to ground. A coaxial cable lead from the electrodes to a Keithley 610B multistage electrometer which was used to measure both streaming currents and potentials. The downstream side of the test cell and the collecting tank were well insulated from the other parts of the apparatus.

3.2. Experimental procedure

The tanks and test cell were cleaned with alconox solution, distilled water and heptane successively, prior to the initial addition of heptane to the system. The ionizing agent was added to the heptane from a stock solution to produce the desired conductivity and the heptane was then pumped through the apparatus to bring about complete mixing. Changes to higher concentrations of ASA #3 did not necessitate cleaning the apparatus.

A filter was mounted in the test cell and both sides of the cell were filled with fluid. The filter was allowed to soak for twenty-four to forty-eight hours with the apparatus fully earthed, before tests were performed. The upstream tank was pressurized and maintained at about 15 psi, and flow rates were adjusted by means of the downstream valve on the test cell. Electrode spacings were set using the micrometers mounted on the cell for this purpose. Flow rates were determined from the average of three measurements of the time required to collect 10 cm^3 of fluid in a buret downstream of the test cell. After any alteration in flow rate or electrode spacing no data was taken for at least five minutes, to allow a new steady state of the system to be attained. Streaming currents and potentials were then measured on the electrometer.

Since it was not a priori clear whether the electrometer had an internal resistance large compared with the resistance of the fluid between the electrodes it was important to determine when a true streaming current (with no significant potential difference developed between the electrodes) and when a true streaming potential (no significant current flow) had been developed. Simultaneous measurements

of current through the electrometer and potential difference across it were made for a variety of internal resistances of the electrometer ranging from 10^8 to 10^{11} Ω. In addition, potentials alone were measured at a meter resistance of 10^{14} Ω. By measuring currents and potentials over this range of meter resistances it was possible to obtain a complete current potential curve for given flow conditions and to establish values of zero-potential streaming currents and zero-current streaming potentials.

At each of the four nominal ASA #3 concentrations at which experiments were performed, tests were carried out using one or more filters. The variations of streaming currents and potentials with flow rate, electrode spacing, external resistance and fluid conductivity were recorded. Some experiments were also performed to investigate the effect of filter thickness on charging characteristics by mounting two or three filters in intimate contact with each other. Two nominal pore radii and a wide range of Debye ratios were tested.

Each filter was used for only one experiment at one conductivity. Transient phenomena were observed (Appendix 9) but not specifically investigated. Some considerable effort was in fact directed to ensure that truly steady state conditions were attained before data was taken. The possibility that the fixed charge within the filter could change with the period of immersion of the filter in the hydrocarbon fluid was suggested by the nature of the transient currents measured when a fresh filter was tested immediately after being mounted. For

this reason filters were soaked for some time in the fluid before measurements were made. Considerable repitition of some experiments was still required before consistent results could be obtained. Only those results are presented which were repeatable and consistent.

It was noticed that when high pressure drops occurred across a filter nitrogen bubbles appeared in the fluid immediately downstream of the filter. Bubble formation could significantly affect filter behavior at higher flow rates which require increased driving pressures. Care was taken in our experiments to operate at low driving pressures and thereby avoid this problem.

3.3 Results

The results of our experiments are in good agreement with the theoretical solutions we have derived. A self consistent analysis of all experimental data has been performed using the high charge ratio theoretical solution (Eq. (16),Eq. (26)-(28)). The data could also have been correlated using the low charge ratio solution (Eq.(16), Eq.(25), Eq. (28)) by postulating that the fixed charge was acquired by the filter in direct proportion to the conductivity of the feed solution. The absence of a definitive value for the diffusion coefficient of the ASA #3 ions gives rise to the uncertainty as to which theoretical solution should be applied. However, by assuming a reasonable value for this diffusion coefficient the experimental data will be shown to be in agreement with the high charge ratio solution, without recourse to additional assumptions.

A second possible source of uncertainty is the fact that the Debye length of the fluid within the filter will differ from that of the neutral fluid outside the filter when the charge ratio is high*. Since no direct measurement of the charge ratio could be made the problem cannot be fully assessed. The theory is not, however, explicitly dependent on the Debye ratio as long as this ratio is large compared with unity.

---

* It can easily be shown that for high charge ratios ($\rho^* >> 1$) :

$$\lambda_D^*\ \text{inside filter} \sim \frac{\lambda_D^*\ \text{outside filter}}{\sqrt{\rho^*}} \quad \text{(See Appendix 2)}$$

The parameters of the experiments conducted are shown in Table 2. In all cases Debye ratios based on bulk fluid conductivity were large, varying from about 10 to 80 for the two filter types used. Peclet numbers for most data points were in the range $.2 < Pe < 2$, exceeding unity at the highest flow rates in all experiments. We note, however, that no significant deviations from the theory were observed for Peclet numbers as high as 6. Electrode spacings were in every case large compared with filter thicknesses. In addition, the conductivity of the solid constituent of the filters was determined to be negligible in comparison with the fluid conductivities used (Appendix 8). In these two limits the theoretical solutions for high charge ratios can be simplified to:

$$\Delta\phi_{e1\ e2} = \phi_o - IR_e \tag{16}$$

$$\frac{zF\phi_o}{RT} = \frac{VL_f}{D} \tag{29}$$

$$R_e = \frac{L_e}{A\sigma_o} \tag{30}$$

$$L_f = Th \tag{19}$$

$$V = \frac{QT}{\varepsilon A} \tag{4}$$

where $\Delta\phi_{e1\ e2}$ is the streaming potential developed between the electrodes.

Exact values for the ionic charge number z and the ion diffusion coefficient D of the ASA #3 ions and for the filter tortuosity T were not known, and thus the value of T^2/zD, needed to evaluate ϕ_o (Eq.(29)), could not be directly obtained. However, all data could be correlated with

$T^2/zD = 3.9 \times 10^5$ sec/cm^2 , which could correspond to $T = 1.6$, $z = 1$ and $D = .65 \times 10^{-5}$ cm^2/sec. For a wide class of porous materials $T \approx 1.6$ (Appendix 3) and z is probably unity since we are dealing with a liquid of very low permittivity. $D = .65 \times 10^{-5}$ cm^2/sec. is a very reasonable value for the diffusion of relatively high molecular weight ions in hydrocarbon fluids (Appendix 7). All lines included in the presentation of the data (Fig. (7) to Fig. (13)) which are drawn from theory are therefore based on $T^2/zD = 3.9 \times 10^5$ sec/cm^2 .

Figs. (7)-(11) indicate the types of experiments performed and the good agreement of the data with our theoretical solutions. Fig. (7) is a plot of zero-current streaming potentials generated across one, two or three filters in intimate contact versus reduced flow rates. As predicted by Eq. (16) a linear dependence is obtained; furthermore the slope of the data agrees well with the theory. Streaming potentials were found to be independent of electrode spacing as expected. A corresponding plot of zero-potential drop streaming currents versus reduced flow rates (Fig. (8)) also agrees well with the theory. Streaming currents were found to be directly dependent on reciprocal electrode spacing as shown in Fig. (9).

The validity of the current potential relation specified by Eq. (16) was further tested by varying the external resistance R_{ext} between the electrodes, and thereby obtaining complete current-potential curves for given flows. Figs. (7) and (8) correspond to cases of $R_{ext} \approx \infty$ ($R_{ext} >> R_e + R_f$) and $R_{ext} \approx 0$ ($R_{ext} << R_e + R_f$) respectively. Fig. (10) includes experimental data for intermediate values of R_{ext} . Lines drawn from the theory included in Fig. (10) are computed as functions of R_{ext} by applying Ohm's law to the external circuit.

Fig. (11) shows the changes in streaming currents that resulted from variations in fluid conductivity. This increase in the magnitude of the streaming current with fluid conductivity (when the Debye ratio remains large) has been observed by previous investigators[4]. Our theory correctly predicts this rate of increase and specifies the range of parameters for which the dependence should occur in low Peclet number flows.

Experiments of the types described were carried out at four conductivities ranging from $6.9 \times 10^{-12}\ \Omega^{-1}\ cm^{-1}$ to $46.0 \times 10^{-12}\ \Omega^{-1}\ cm^{-1}$ (Table 2) using two filter types. Data on zero-current streaming potentials and zero-potential streaming currents has been reduced to two plots (Fig. (12) and Fig. (13)). These show explicitly the dependence of streaming currents and potentials on flow rates and implicitly confirm the dependence of these variables on fluid conductivity, electrode spacing and filter area.Debye ratios and pore sizes are seen to have no effect on charging characteristics in the ranges of these parameters tested.

As expected the best correlation of data is obtained for the dimensionless streaming potentials versus reduced flow rates shown in Fig. (12). Only two measured variables were required to reduce the streaming potential data - flow rate and filter thickness since other parameters such as fluid temperature and filter area remained relatively invariant. For this reason the correlating factor T^2/zD was evaluated from Fig. (12). The higher scatter of the data in Fig. (13) showing dimensionless streaming currents versus reduced flow rates arises from the additional errors introduced in measuring fluid conductivities and electrode spacings. A certain amount of the scatter in Fig. (12) and Fig. (13) can be attributed to the temperature dependence of the ion diffusion coefficient - an effect tacitly neglected since no correction for it could be made.

4. Discussion of previous experimental work.

A number of investigators have carried out experiments on different facets of electrostatic charging in hydrocarbon filtration. While some direct comparisons between our theoretical solutions and earlier experimental work can be made, most previous studies have neglected to consider two aspects of our theory which we have found to be important. For the purpose of evaluating hazards arising from electrostatic charging an understanding of the complete current-voltage characteristics of a filtering system is required. Our theory predicts this current-voltage interdependence for some simple flow conditions. Most other work, however, has been concerned with the development of streaming currents only. Measurements have been made either by assuring that streaming potentials were negligible when currents were recorded or, in some cases, by simply disregarding the possible effects of a potential difference across the measuring electrodes. A second factor which we consider important is the problem of electrode spacing. It is essential to distinguish between the true charging characteristics of a filter and the streaming currents and potentials which may be measured by electrodes at points distant from the filter. As our present analysis has shown, the fluid regions separating a filter from the electrodes can have a significant effect on apparent charging characteristics. It is difficult to interpret experimental results without a precise knowledge of the geometry and conductivity of these regions and the enclosing pipes or tubing. Unfortunately the importance of electrode spacing has been largely disregarded in previous experimental studies.

Experimental work has been carried out by Gavis and Wagner[3] using heptane containing Shell Antistatic Additive #1 flowing through Millipore filters. Peclet numbers for most of their data points were large compared with unity, bringing their experimental results beyond the immediate scope of our theoretical solutions. Furthermore, Gavis and Wagner did not report electrode configurations and spacing lengths. Only some semi-qualitative comparisons between their experiments and our theory can therefore be made.

Gavis and Wagner concluded that streaming currents were independent of filter thickness, in contrast with our theory and experiments which indicate a linear dependence of streaming currents on filter thickness for low Peclet number filtration. In view of the range of filter thicknesses (h) tested by Gavis and Wagner ($1.00 \times 10^{-2} < h < 1.5 \times 10^{-2}$ cm) and the apparent scatter in their data (about a factor of four variation in streaming currents for given flow conditions) their conclusion seems somewhat tenuous. It is, however, quite possible that when the fluid relaxation length $Pe\lambda_D$ exceeds the effective filter thickness ℓ, streaming currents may depend on this larger characteristic length rather than on the filter thickness which is the governing parameter for low Peclet number flows.

The dependence of streaming currents I on flow velocity V, fluid relaxation time τ_o, fluid conductivity σ_o and diffusion coefficient D obtained by Gavis and Wagner is of the form:

$$I \propto \frac{V^{1\ 3/4}\ \tau_o^{\ 3/4}\ \sigma_o}{D} \sim \frac{V(Pe\lambda_D)}{D}\ \sigma_o \qquad (31)$$

For low Peclet number, high charge ratio flows with large electrode spacings, streaming currents as predicted by Eqs. (16), (29), (30) obey

a relationship of the form:

$$I \propto \frac{V\ell}{D} \sigma_o \qquad Pe << 1 \qquad (32)$$

If for high Peclet number flows the effective filter thickness ℓ is replaced by the fluid relaxation length $Pe\lambda_D$ in Eq. (32), then Eqs. (31) and (32) become equivalent.

Gavis and Wagner have found streaming currents to depend on pore radius according to:

$$I \propto a^{-3/4} \qquad (33)$$

while our theory for large Debye ratio flows requires that streaming currents be independent of pore radius. Since not all of Gavis' and Wagner's data is for large Debye ratio flows it is difficult to comment on this reported dependence. We note, however, that pore radii in their experiments ranged from $.25 \times 10^{-5}$ cm to 4.00×10^{-5} cm. According to their correlating equation this variation in pore size would result in a factor of eight variation in streaming currents for otherwise identical flow conditions - a variation only slightly greater than the scatter in their experimental data.

Leonard and Carhart[4] have conducted experiments on charge generation for aviation fuels containing Shell Antistatic Additive ASA #3 flowing through fiberglass filters. It is again difficult to compare their data with our theoretical solutions because certain parameters essential to our theory were not reported. Filter pore sizes were not given making it impossible to evaluate Debye ratios,and insufficient information was given

on electrode spacings. The substantially higher flow rates required in Leonard and Carhart's "fuel charging apparatus" to give charging currents of the same magnitude as in their "water separometer method" for otherwise equivalent filtering conditions can be attributed to the larger electrode spacing lengths involved in the "fuel charging apparatus". The approximately linear dependence of streaming currents on fluid conductivity for a range of fluid conductivities is consistent with our theory for large Debye ratio flows with significant electrode spacing lengths. Leonard and Carhart found that streaming currents reached a maximum and then decreased as conductivity was further increased: this would be a reflection of the change from large Debye ratio to intermediate and small Debye ratio filtering conditions caused by the increase in fluid conductivity.

Lauer and Antal [5],[6] have performed experiments on charge generation for flows of a variety of hydrocarbons through porous materials. Again filter pore sizes and electrode spacing distances were not reported, making their data difficult to analyze. Many of their experiments on non-uniform flows are beyond the scope of our present solutions. While Lauer and Antal suggest that streaming currents are independent of filter thickness (and draw attention to the agreement with Gavis' and Wagner's similar conclusion) they present only slight experimental justification for this observation.

3. Concluding Remarks

A theory for charging phenomena in hydrocarbon filtration has been presented. The theory is based on a relatively simple model for filter geometry and electrostatic structure wherein the filter is assumed to consist of tortuous pores, the interior surfaces of which acquire a uniform fixed charge when in contact with a weak electrolyte.

The solutions we have obtained for charging through filters lack generality in that they restrict flows to small Peclet numbers. Many practical cases of fuel filtration will not meet this requirement and it is therefore important to extend the theory and remove this restriction. We note here that for low charge ratio flows our solutions can be shown to be generally valid without regard to the magnitude of the Peclet number provided that a length of fluid at least equal to the relaxation length (as defined in Appendix 1) separates the downstream side of the filter from any conducting surfaces or electrodes. For high charge ratio flows the model must be altered to take into account the charge cloud extension and attenuation which occurs at high Peclet numbers. Theoretical solutions for flows where the fluid reaches electrodes before complete charge relaxation occurs are also required.

The present theory should be further generalized to remove the large Debye ratio restriction presently imposed. This would allow the model to be applied to higher conductivity fluids or to filters of larger pore radii. As a first approximation we can treat this aspect of the charging problem by assuming laminar flow through cylindrical pores with the charge distribution across a pore diameter determined by the Debye ratio and wall

charge (as discussed in Appendix 2).

Transient charging phenomena which occur for unsteady flow conditions and time-varying filter properties also require further study. Substantial modifications in our model to allow for the electric capacitance of the double-layers inside and downstream of the filter, and an understanding of the kinetics of fixed charge formation are required.

Finally, if the theory is to be used for quantitative predictions in engineering situations one must have available as handbook information the fixed charge densities for the typical filter material and permeant fluid combinations expected in practice. Such data must still be generated by running tests on a variety of filter materials and hydrocarbon liquids.

While considerable further development of our solutions is required the strength of our model has been established. A theoretical treatment of charging through filters in terms of physically meaningful parameters has been formulated without recourse to empirical correlation.

Table 1

Summary of Theoretical Solutions

$L_e = L_1 + L_2$

$L_f = Th$ (See Fig. 5)

$V = QT/\varepsilon A$

$$\rho_o = \frac{\sigma_o RT}{zFD}$$

$$\rho^* = \left|\bar{\rho}_f/\rho_o\right|$$

Solutions are valid when $Pe << 1$, $\lambda_D/\ell << 1$ and $\bar{\rho}_f$ is uniform in the filter.

For one dimensional flow through two electrodes e_1 and e_2 separated by a filter the streaming potential developed between the electrodes is:

$$\Delta\phi_{e_1\, e_2} = \phi_o - I(R_f + R_e)$$

$$Re = \frac{L_e}{A\sigma_o} \qquad R_f = \frac{L_f}{A\sigma_f}$$

low wall charge $\rho^* << 1$

$$\phi_o = -\frac{V\rho_f \varepsilon L_f}{\sigma_s}$$

$$\sigma_f \approx \varepsilon\sigma_o + (1-\varepsilon)\sigma_s$$

high wall charge $\rho^* >> 1$

$$\phi_o = -\frac{VL_f \bar{\rho}_f \varepsilon L_f}{\sigma_f} \approx \frac{RT}{zF} \frac{VL_f}{D + (\frac{1-\varepsilon}{\varepsilon})(\frac{\sigma_s RT}{zF\rho^*})}$$

$$\sigma_f \approx \varepsilon\sigma_o\rho^* + (1-\varepsilon)\sigma_s$$

Table 2

Run #	Temperature ^{o}C	Filter Type	Number of Filters	Total Filter Thickness x 10^{2} cm	Fluid Conductivity x $10^{12} \Omega^{-1} cm^{-1}$	λ_D^* (1)	Maximum Value of Pe (2)
1	26.8	PH	1	1.5	7.0	27	5.9
2	23.6	VC	1	1.3	6.9	81	6.6
3	25.5	VC	1	1.3	15.4	54	6.5
4	28.2	PH	1	1.5	16.2	18	3.1
5	25.5	PH	1	1.5	15.3	18	3.4
6	23.0	PH	3	4.5	15.2	18	1.3
7	23.0	PH	2	3.0	15.2	18	3.0
8	25.0	PH	1	1.5	26.2	14	3.1
9	23.6	VC	1	1.3	26.0	40	1.4
10	24.4	VC	1	1.3	46.0	30	1.9

(1) Debye ratios are calculated from the bulk fluid conductivity and the nominal pore radius assuming $D = .65 \times 10^{-5}$ cm^2/sec and $\varepsilon_r = 1.97$.

(2) Peclet numbers are calculated from the Debye length based on bulk fluid conductivity with $T^2/zD = 3.9 \times 10^5$ sec/cm^2 and $z = 1$.

Table 3

Liquid	Formula	Relative Permitivity	Conductivity of Pure Solvent Ω^{-1} cm^{-1}
carbon tetrachloride	CCl_4	2.24	4×10^{-18}
ethyl ether	$C_4H_{10}O$	4.33	$< 4 \times 10^{-13}$
pentane	C_5H_{12}	1.8	$< 2 \times 10^{-10}$
nitrobenzene	$C_6H_5NO_2$	36.1	5×10^{-9}
benzene	C_6H_6	2.28	$< 1 \times 10^{-18}$
n-hexane	C_6H_{14}	1.87	$< 1 \times 10^{-18}$
n-heptane	C_7H_{16}	1.97	$< 1 \times 10^{-13}$
m-xylene	C_8H_{10}	2.37	$< 1 \times 10^{-15}$
quinoline	C_9H_7N	9.0	16×10^{-9}
nonane	C_9H_{20}	1.96	$< 17 \times 10^{-9}$

Source: International Critical Tables

Table 4

Filter Type	Mean Pore Diameter $\times 10^4$ cm	Thickness $\times 10^4$ cm	Porosity
P H	$0.30 \pm .02$	150 ± 10	.77
VC	$0.10 \pm .008$	130 ± 10	.74

Source: Millipore Catalogue MC/1[30]

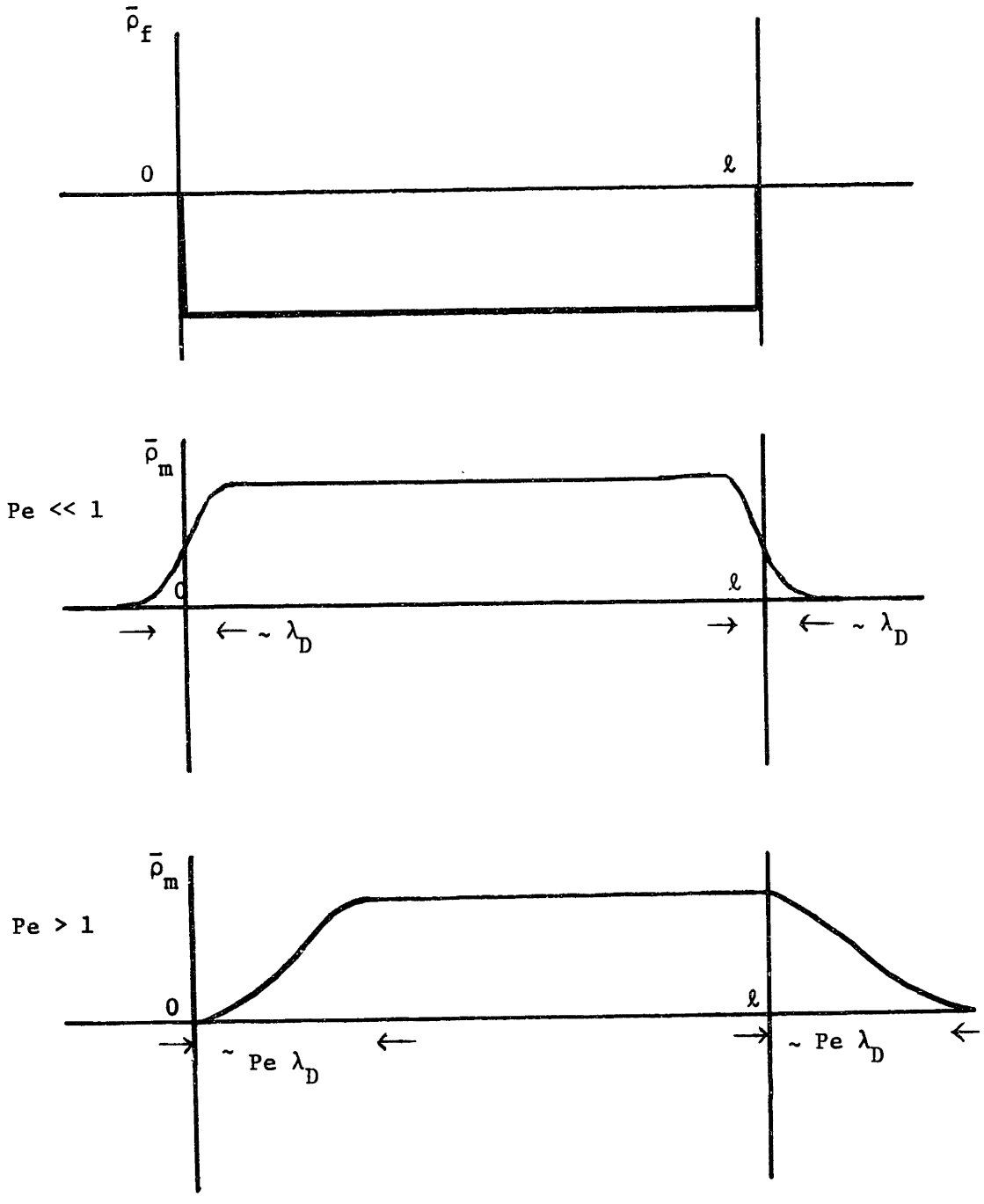

Fig. (1) Fixed and mobile charge distributions in a long cylindrical pore for large Debye ratio flows.

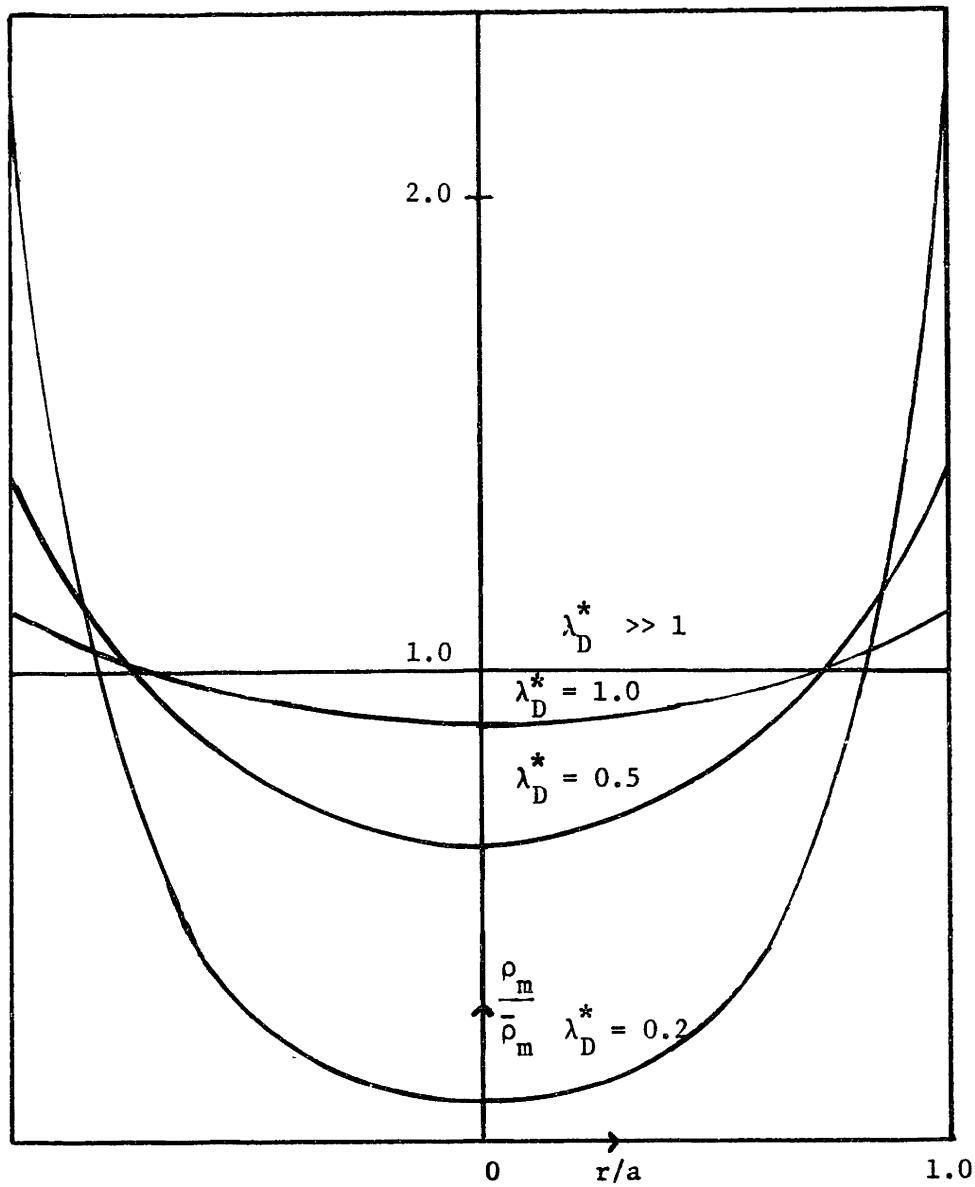

Fig. (2) Effect of Debye ratio on radial charge distribution in a long cylindrical pore. Curves are applicable for low wall charges and for fluids at rest or moving with fully developed velocity profile.

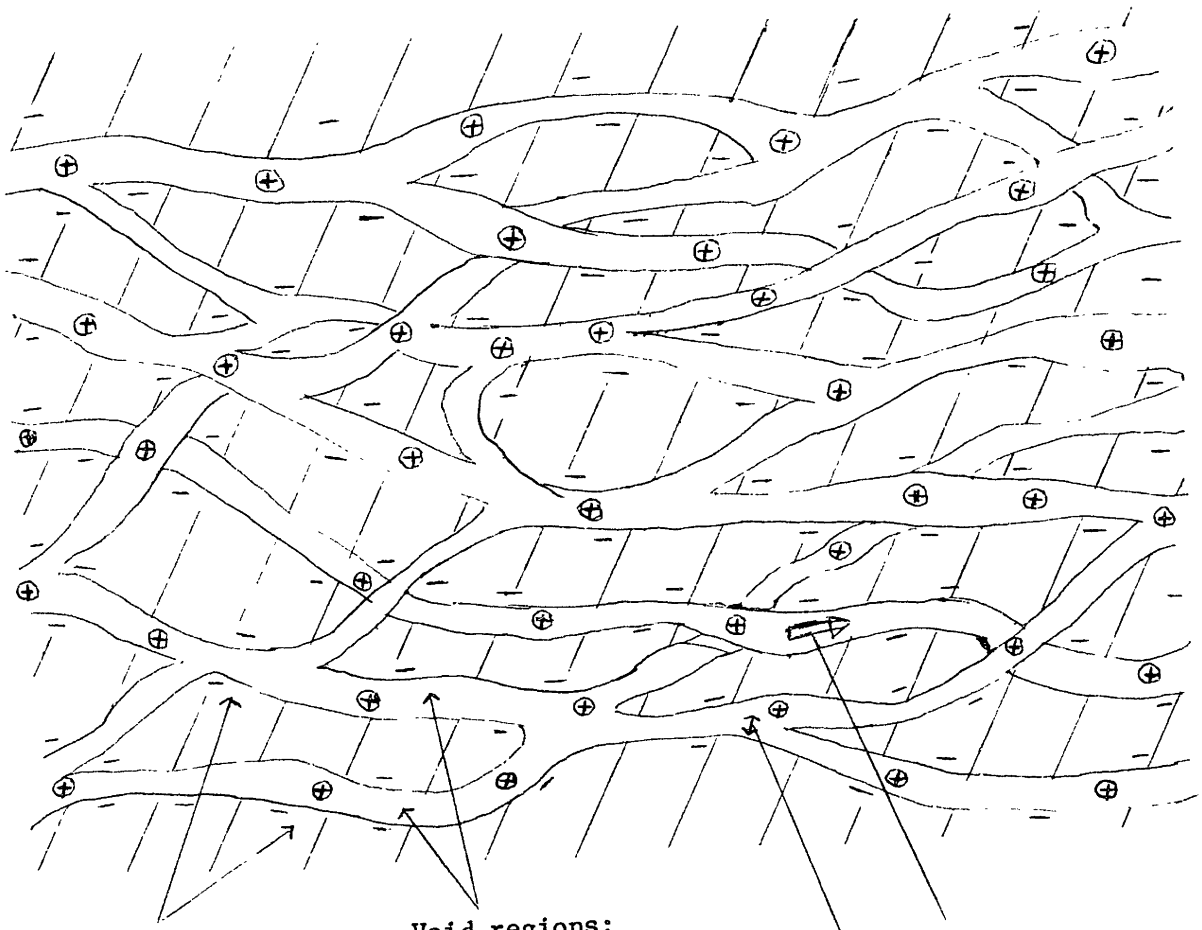

quasi-neutrality:

$$\bar{\rho}_f + \bar{\rho}_m = 0$$

Fig. (3) Model of the electrostatic structure of a filter.

Definition of tortuosity:

$$\int_{I}^{II} d\underline{\ell} \approx \int_{1}^{2} d\underline{\ell} \equiv Th$$

Current flux equation:

$$\int_{1}^{2} \underline{j} \cdot d\,\underline{\ell} = -\bar{\rho}_f \int_{1}^{2} \underline{V} \cdot d\underline{\ell} - \sigma_m \int_{1}^{2} d\phi$$

Integrated flux equation:

$$j\,Th = -\bar{\rho}_f\,V\,Th - \sigma_m\,\Delta\phi_{12}$$

Fig. (4) Characteristic particle path through a filter.

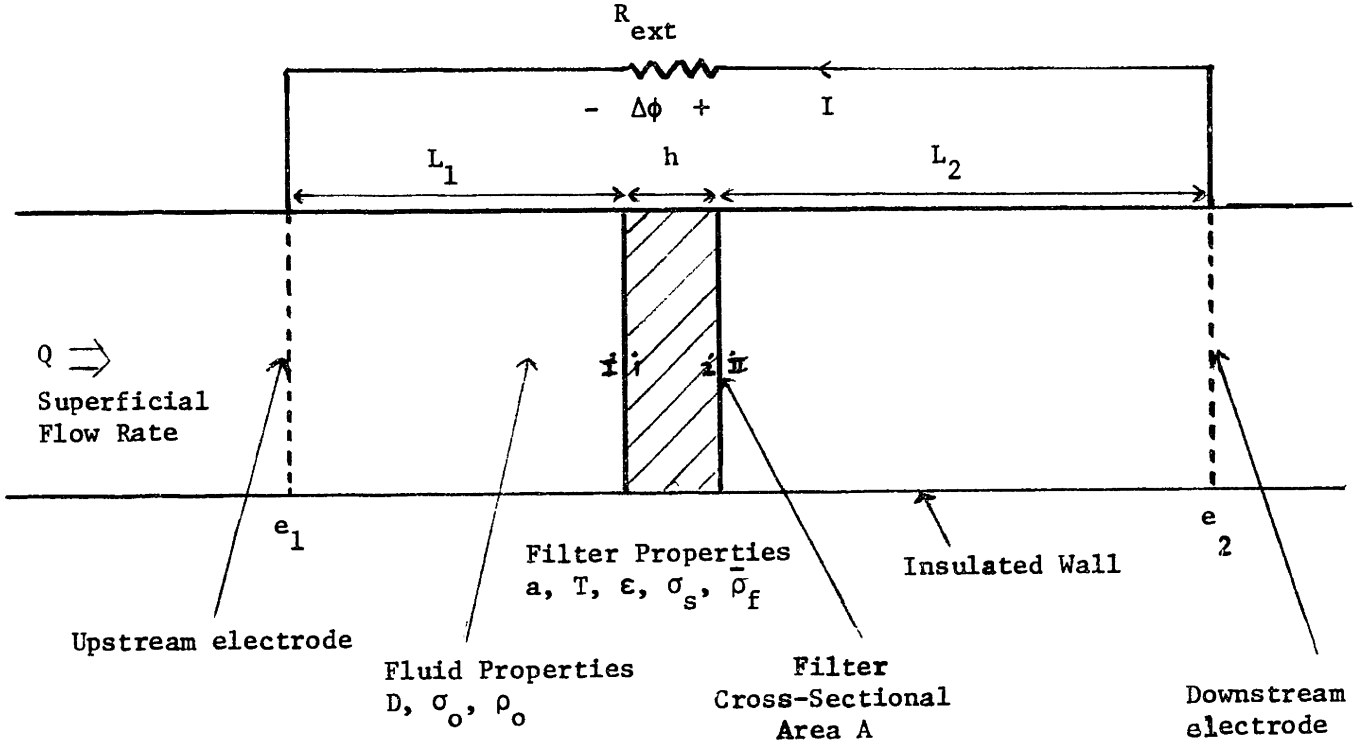

Fig. (5) Filter and electrodes for one dimensional flow.

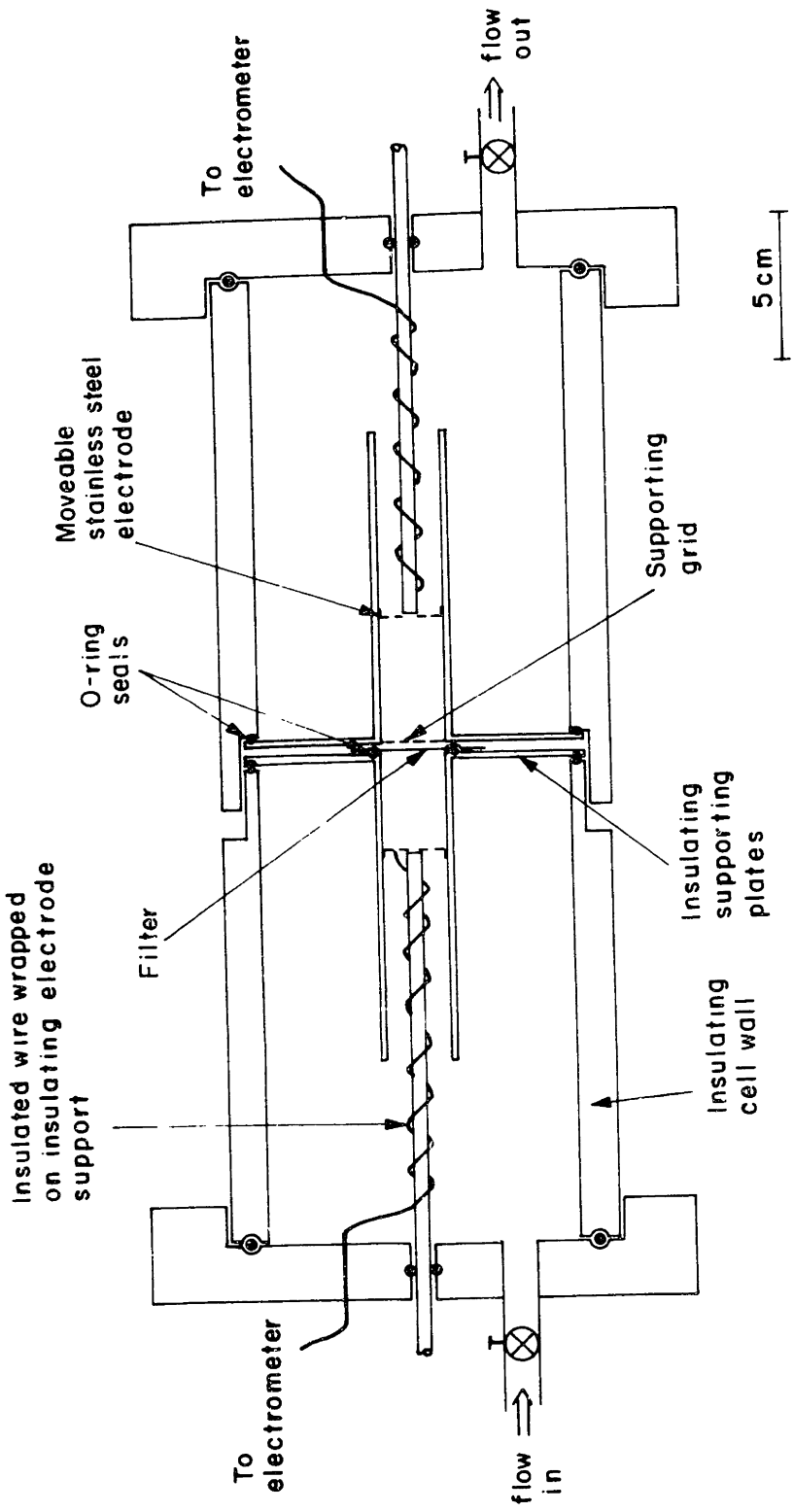

Fig. (6) Test cell.

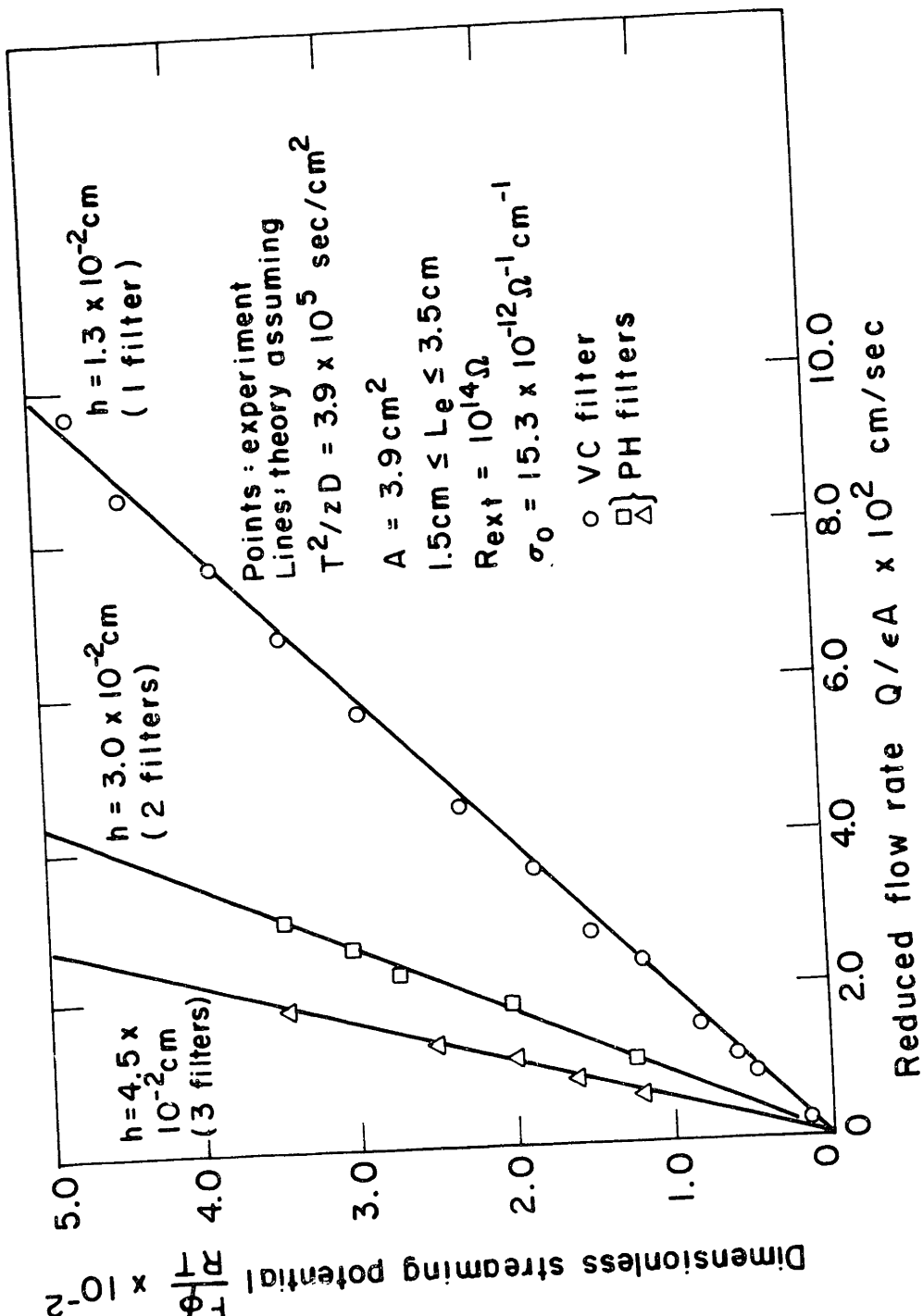

Fig. (7) Dimensionless streaming potential (potential at zero current) as a function of reduced flow rate for one, two and three filters in series.

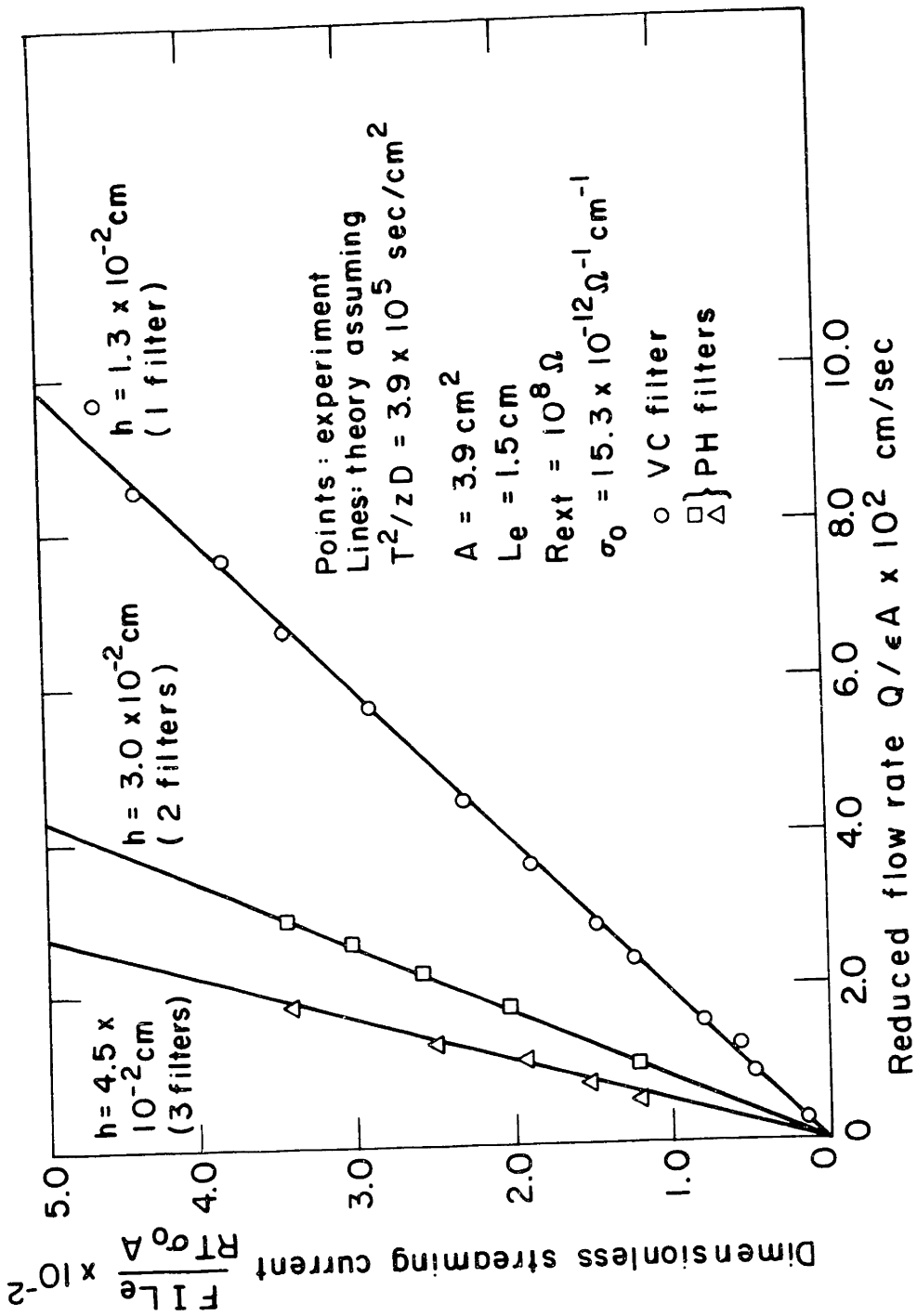

Fig. (8) Dimensionless streaming current (current with electrodes shorted) as a function of reduced flow rate for one, two and three filters in series.

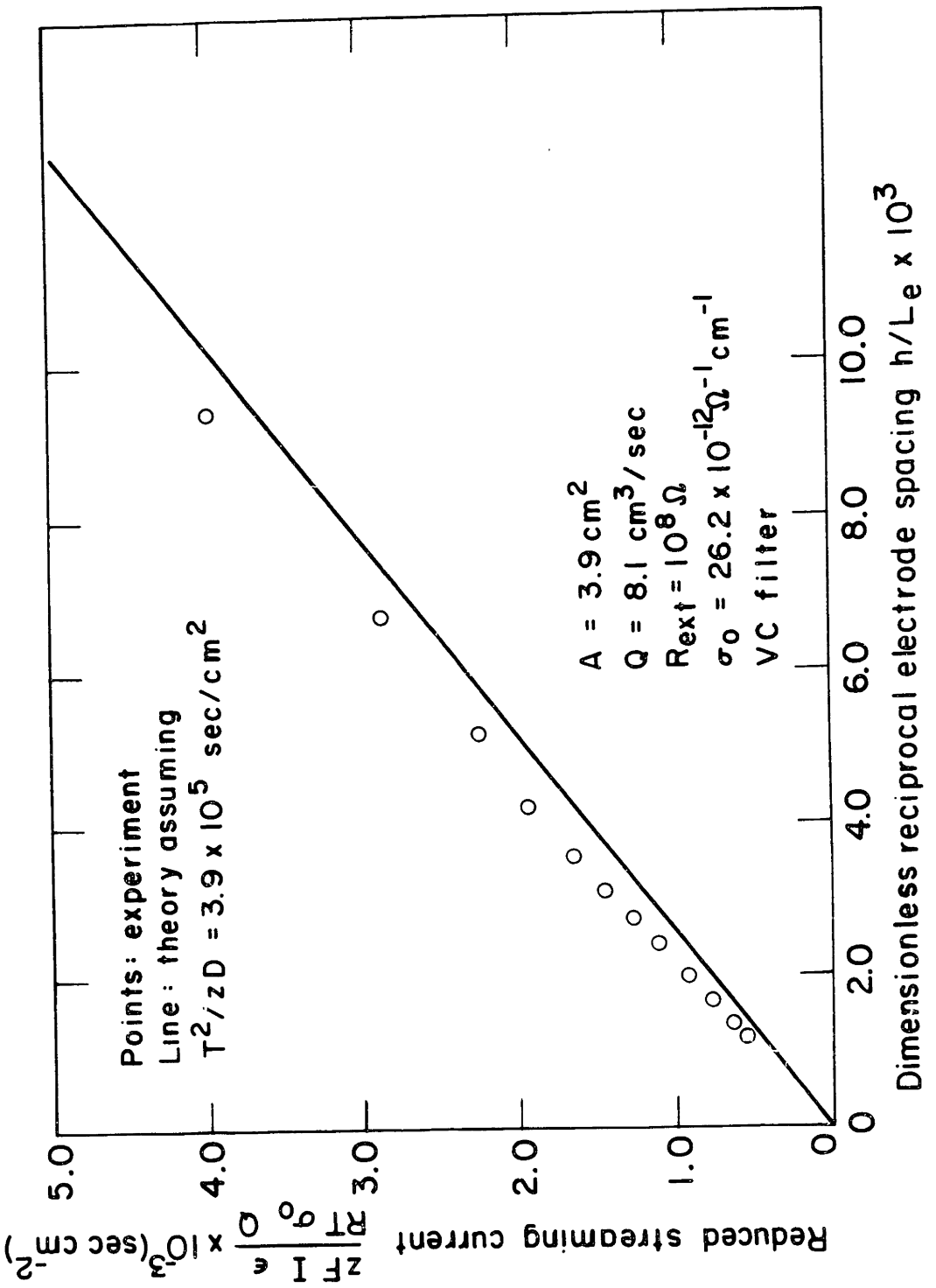

Fig. (9) Reduced streaming current (current with electrodes shorted) as a function of reciprocal electrode spacing.

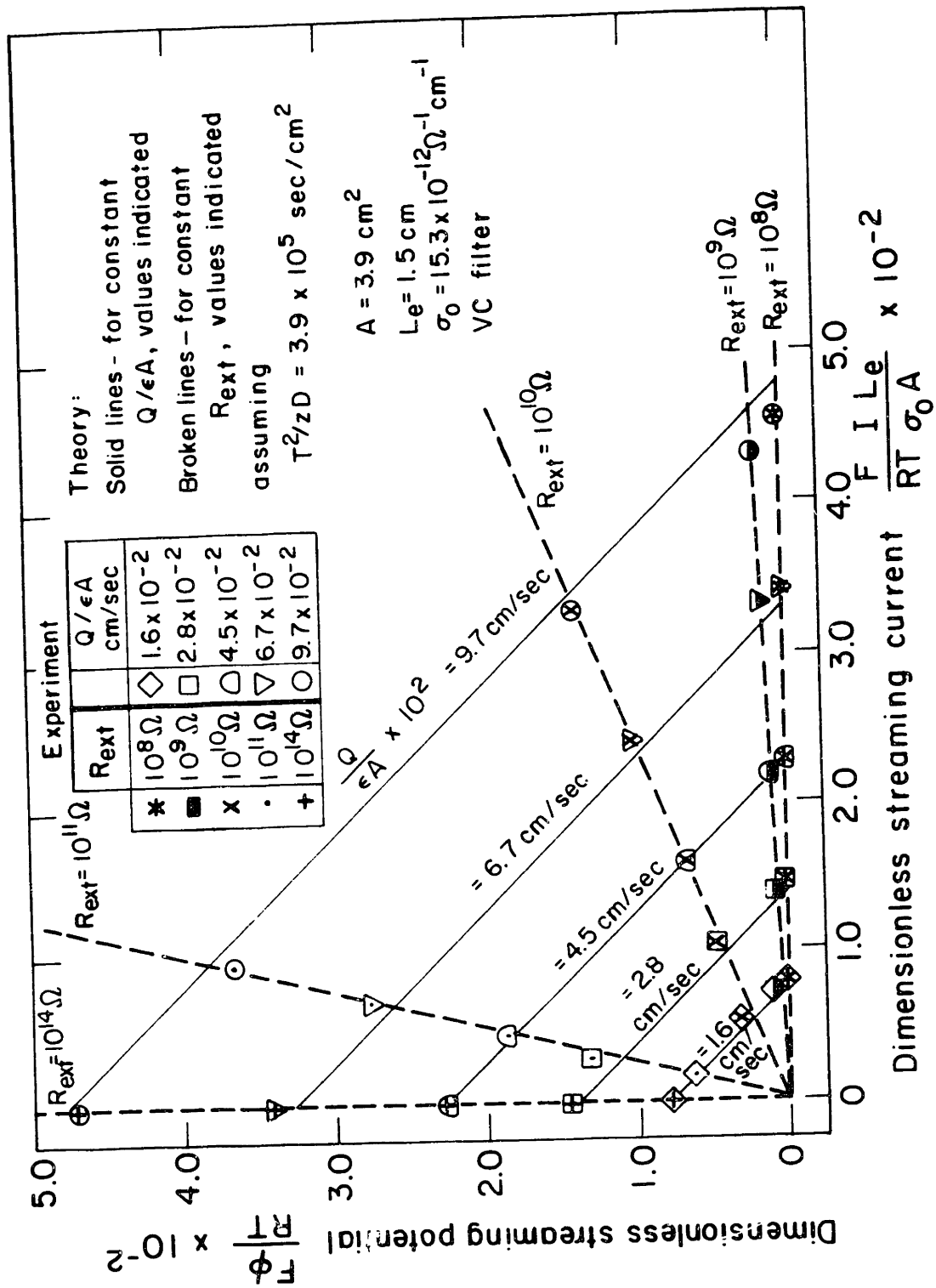

Fig. (10) Dimensionless potential as a function of dimensionless current for various flow rates and external resistances.

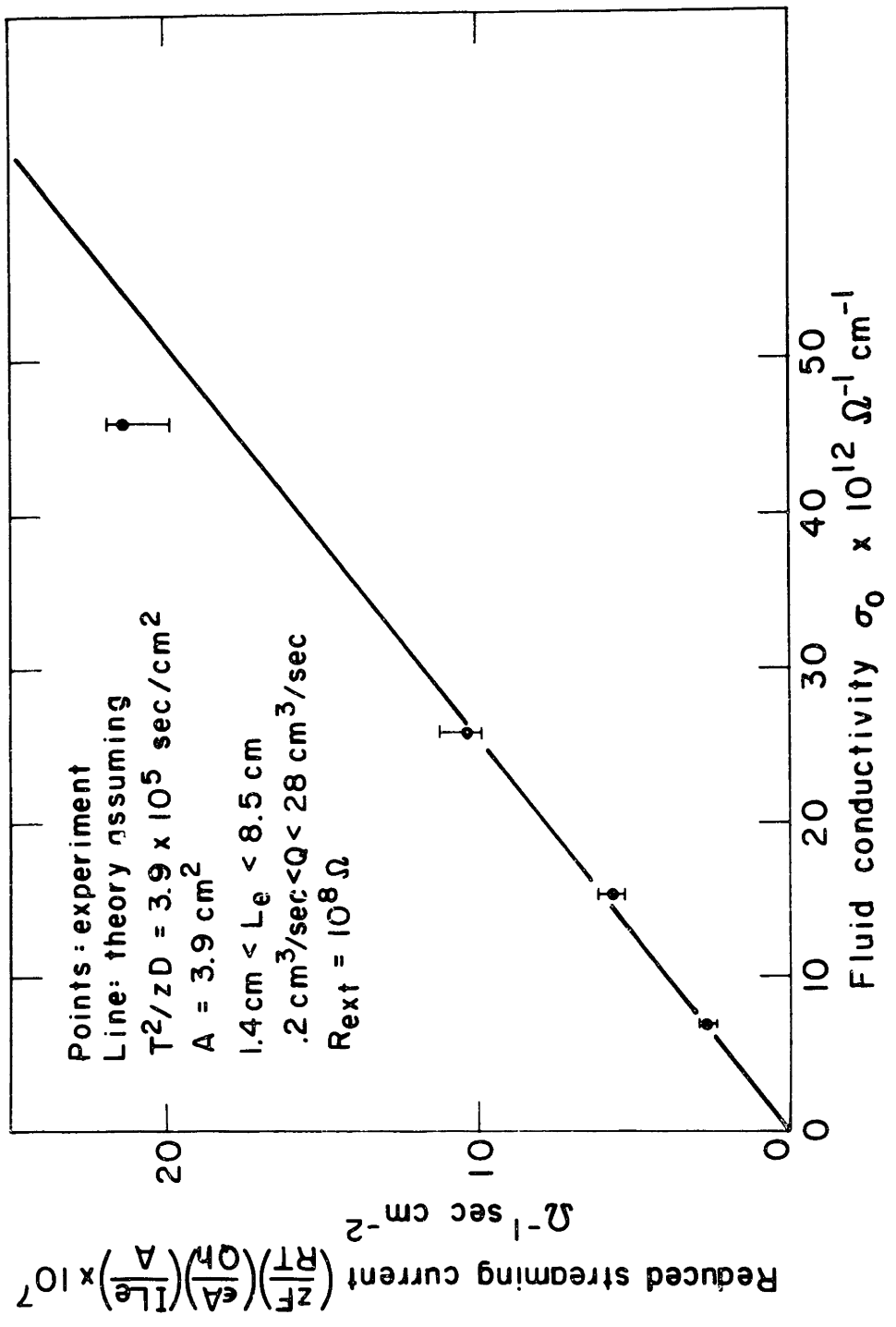

Fig. (11) Reduced streaming current (current with electrodes shorted) as a function of fluid conductivity.

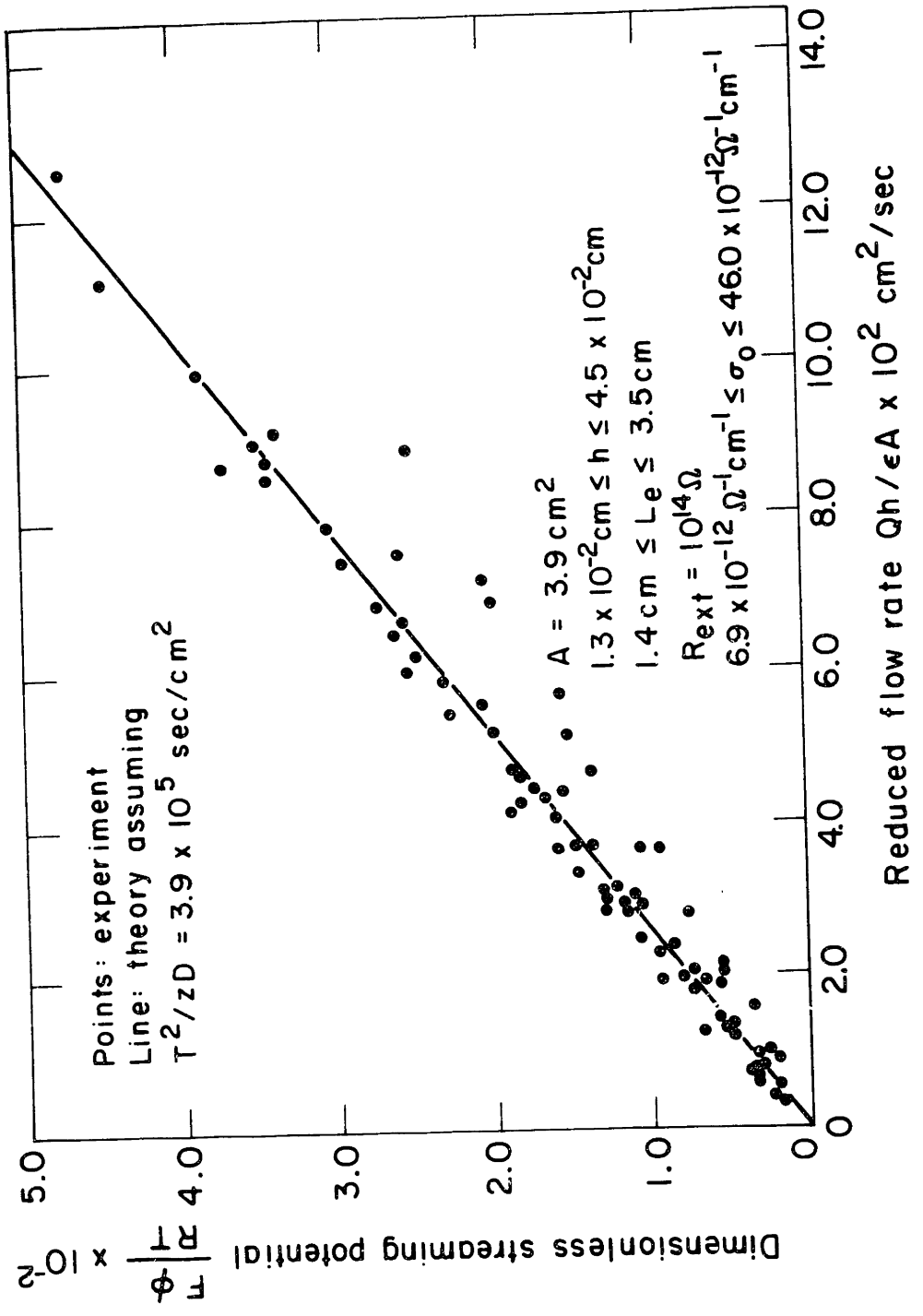

Fig. (12) Dimensionless streaming potential (potential at zero current) as a function of reduced flow rate.

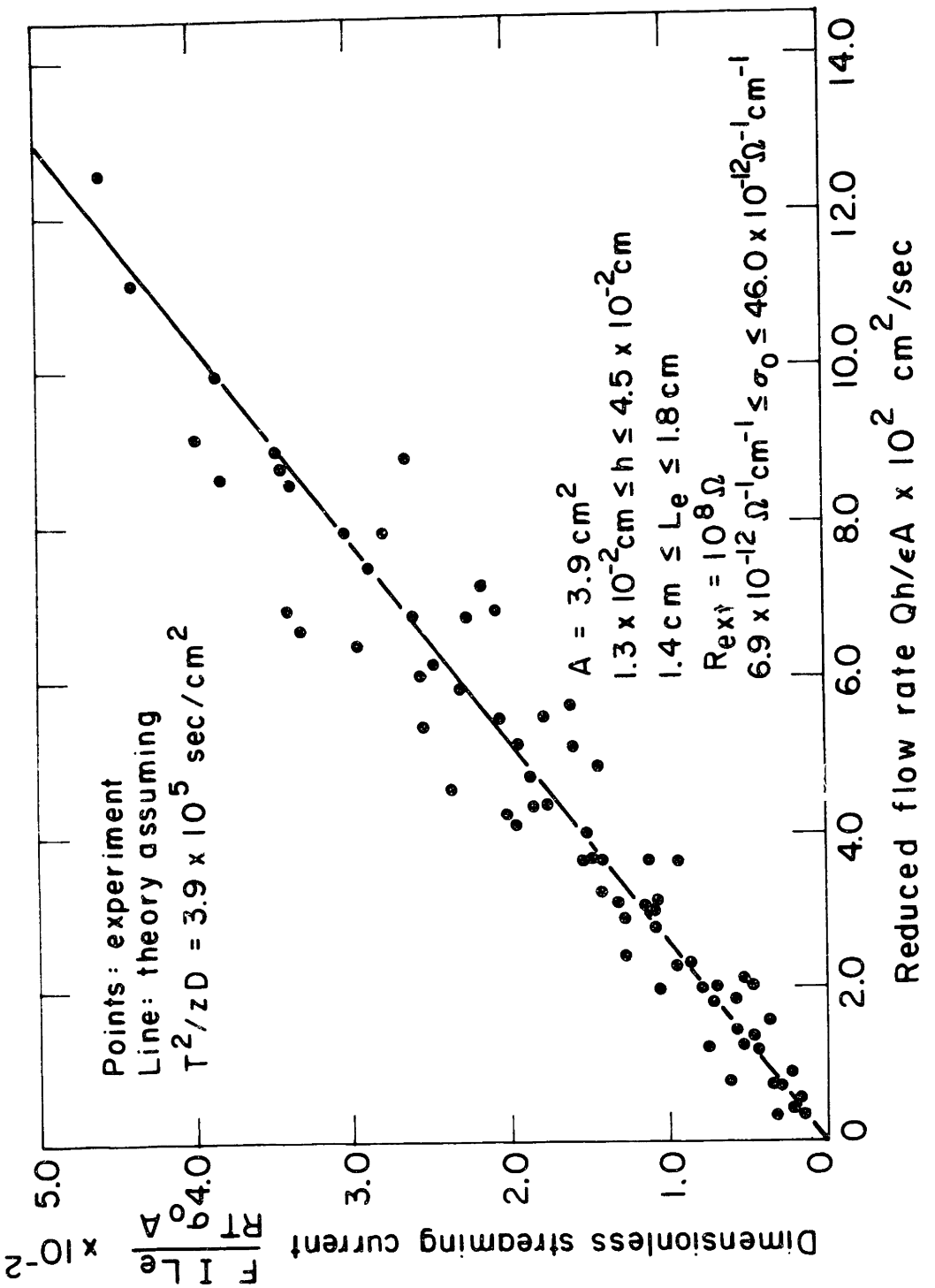

Fig. (13) Dimensionless streaming current (current with electrodes shorted) as a function of reduced flow rate.

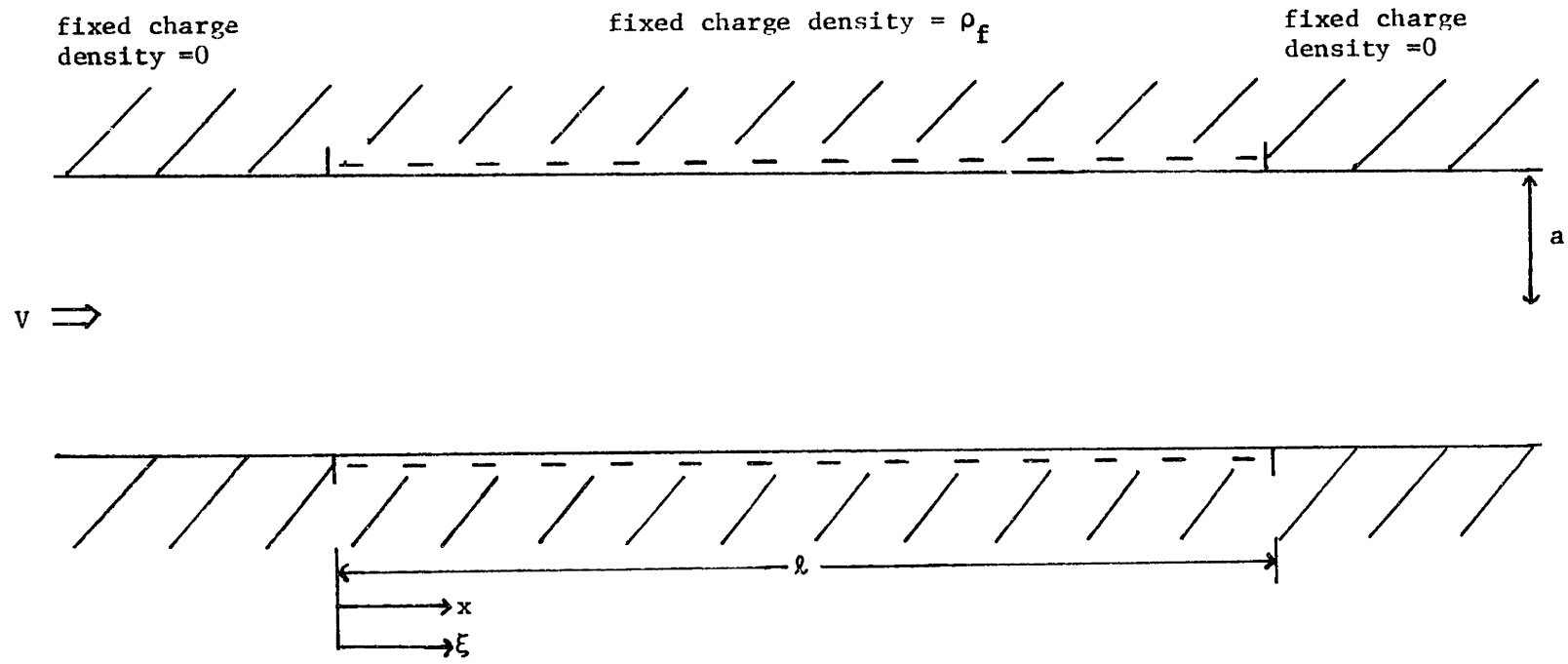

Fig. (14) Charge relaxation for large Debye ratio flow through a cylindrical pore.

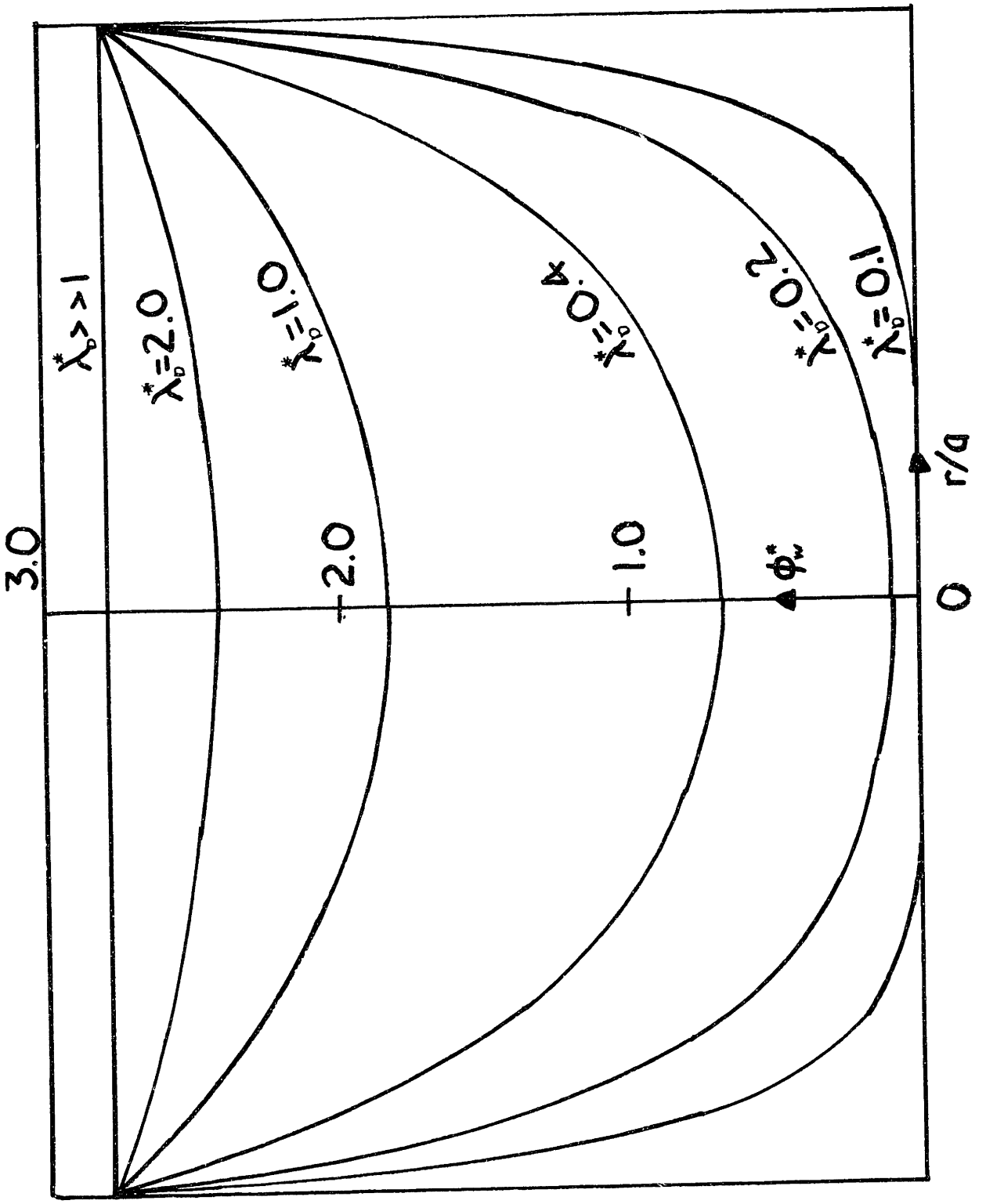

Fig. (15) Dimensionless radial potential distribution across a cylindrical pore for different Debye ratios and a fixed wall potential ($\phi_w^* = 2.79$) .

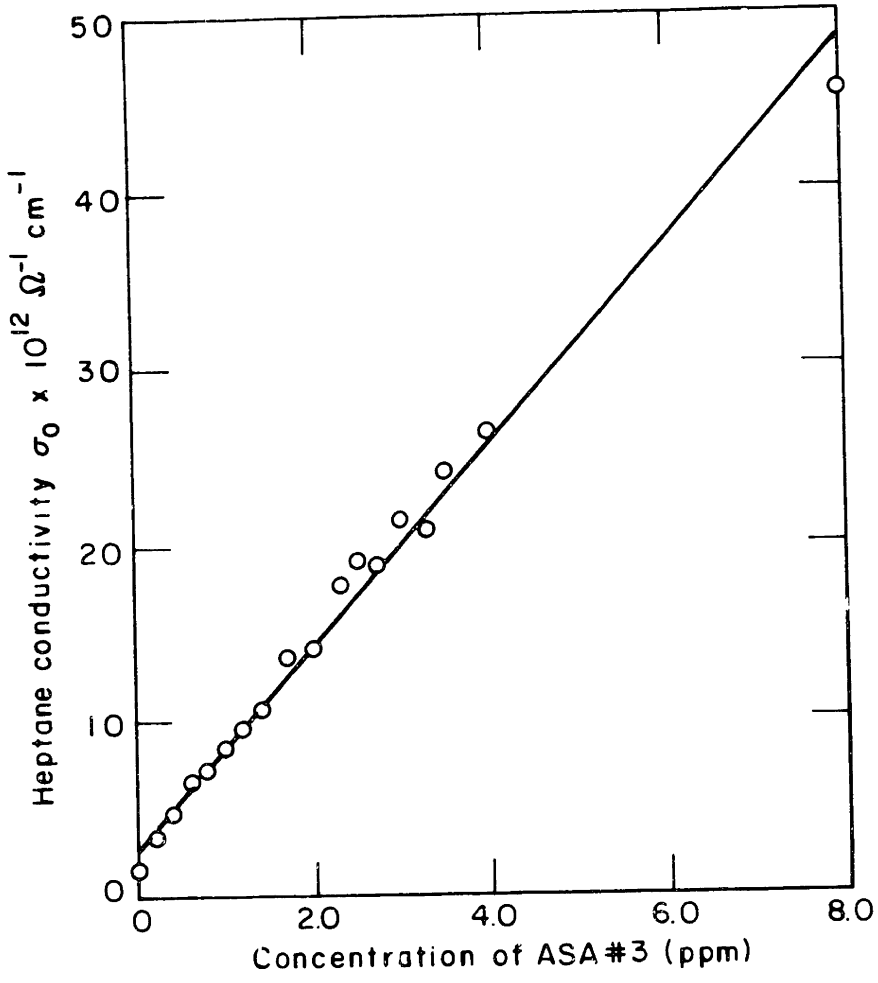

Fig. (16) Heptane conductivity as a function of the concentration of Shell Antistatic Additive #3.

Appendix 1

Charge relaxation for one-dimensional large Debye ratio flow

All electrolytes are characterized by a relaxation time which depends on the fluid and ion properties and ion concentrations in the electrolyte. This time is a measure of how quickly the fluid will conform with imposed electrostatic boundary conditions. Specifically, the relaxation time is a decay constant fot the discharge of a hypothetical condenser constructed with the electrolyte as the dielectric medium[1].

If an electrolyte flows past a solid surface and convects the mobile charge existing adjacent to the surface a potential will be developed in the fluid to prevent the indefinite displacement of this mobile charge. The distance over which this potential develops is the relaxation length, given by the product of the fluid flow velocity and relaxation time.

The charge relaxation equation is obtained by combining the Nernst-Planck flux equation (Eq. (5)) with the current and mass continuity equations and Poisson's equation (see for example Gavis and Kozman [12]). In one dimension it can be written as*:

$$\frac{d^2\rho}{dx^{*2}} - Pe\,\frac{d\rho}{dx^*} - \rho = 0 \qquad \text{(A1.1)}$$

$$x^* = x/\lambda_D \qquad \text{(A1.2)}$$

$$Pe \equiv \frac{V\lambda_D}{D} \qquad \text{(A1.3)}$$

---

* The value of λ_D is assumed to be constant - this will be the case when charge densities in the fluid are low. (See Appendix 2)

Pe >> 1

$$\rho_m = \frac{\rho_f}{Pe^2}\left(-e^{-Pe(x^* - \ell^*)} + e^{-Pe\, x^*}\right) \approx 0 \qquad x^* \leq 0 \tag{A1.8}$$

$$\rho_m = \rho_f \left(e^{\frac{-x^*}{Pe}} - 1\right) \qquad 0 < x^* < \ell^* \tag{A1.9}$$

$$\rho_m = \rho_f \left(e^{-x^*/Pe} - e^{(\ell^* - x^*)/Pe}\right) \qquad \ell^* \leq x^* \tag{A1.10}$$

where $\ell^* = \ell/\lambda_D$.

Fig. (1) shows the charge distributions corresponding to Eq. (A1.5) - Eq. (A1.10). The derivation of these solutions follows.

Solution for low Peclet number flows

An order of magnitude analysis of Eq. (A1.1) indicates that the second term of the equation becomes negligible in comparison with the other two terms when $Pe << 1$. We therefore seek solutions of the form:

$$\rho = Ae^{x^*} + Be^{-x^*} \tag{A1.11}$$

with A and B undetermined constants. Upstream of the charged section of the pore ($x^* \leq 0$ in Fig. (14)) the fixed charge density is zero, and the mobile charge density must tend to zero at large distances. A similar argument is valid for regions downstream of the charged section of the pore. Thus:

$$\rho_m = Ae^{x^*} \qquad x^* \leq 0 \tag{A1.12}$$

$$\rho_m = Be^{-x^*} \qquad \ell^* \leq x^* \tag{A1.13}$$

Within the charged section we seek a symmetric solution of the form:

$$\rho_m + \rho_f = C(e^{-x^*} + e^{x^* - \ell^*}) \qquad 0 < x^* < \ell^* \tag{A1.14}$$

A symmetric solution must be valid since boundary conditions are symmetric and the convective term of Eq. (A1.1) has been neglected. At points $x^* = 0$ and $x^* = \ell$ the mobile charge density must be continuous, and hence we obtain:

$$\rho_m = C\left[e^{x^*} + e^{\ell^* - x^*}\right] - \rho_f e^{x^*} \qquad x^* \leq 0 \tag{A1.15}$$

$$\rho_m = C\left[e^{-x^*} - e^{x^* - \ell^*}\right] - \rho_f \tag{A1.16}$$

$$\rho_m = C\left[e^{-x^*} + e^{\ell^* - x^*}\right] - \rho_f e^{\ell^* - x^*} \tag{A1.17}$$

Next we impose overall neutrality as required by Eq. (A1.4):

$$\int_{-\infty}^{0} \left\{ C\left[e^{x^*} + e^{\ell^* - x^*}\right] - \rho_f e^{x^*} \right\} dx^*$$

$$+ \int_{0}^{\ell^*} \left\{ C\left[e^{-x^*} + e^{x^* - \ell^*}\right] - \rho_f \right\} dx^*$$

$$+ \int_{\ell^*}^{\infty} \left\{ C\left[e^{-x^*} + e^{\ell^* - x^*}\right] - \rho_f e^{\ell^* - x^*} \right\} dx^* \tag{A1.18}$$

$$+ \rho_f \ell^* = 0$$

which gives:

$$C = \frac{\rho_f}{2} \tag{A1.19}$$

Substituting this value for C into Eq. (A1.15) - Eq. (A1.17) we obtain the charge relaxation equations for low Peclet number flows, Eq. (A1.5) - Eq. (A1.7).

Solution for high Peclet number flows

If we consider a high Peclet number flow $(Pe >> 1)$ through a surface array of fixed charges (located at the origin) with fixed charge density ρ_f then solutions to Eq. (A1.1) are easily found:

$$\rho_m = -\frac{\rho_f}{Pe} e^{Pe\, x^*} \qquad x^* < 0 \tag{A1.20}$$

$$\rho_m = -\frac{\rho_f}{Pe} e^{-x^*/Pe} \qquad 0 \leq x^* \tag{A1.21}$$

Since Eq. (A1.1) is linear and homogeneous we can obtain the solution for high Peclet number flow through a pore bearing a fixed charge over a section of finite length by superposition of the solution for flow through a surface. Introducting a dummy variable ξ^* to denote dimensionless distance measured along the charged length of the pore, we obtain by superposition:

Upstream of charged section

$$\rho_m = \int_o^{\ell^*} \frac{-\rho_f}{Pe} e^{Pe(\xi^* - x^*)} d\xi^* \qquad x^* \leq 0 \tag{A1.22}$$

$$\rho_m = \frac{\rho_f}{Pe^2} \left(-e^{-Pe(x^* - \ell^*)} + e^{-Pex^*} \right) \tag{A1.23}$$

$$\approx 0 \qquad x^* \leq 0 \tag{A1.24}$$

Downstream of the charged region of the pore

$$\rho_m = \int_o^{\ell^*} \left(\frac{-\rho_f}{Pe} e^{-\frac{x^* - \xi^*}{Pe}} \right) d\xi^* \qquad \ell^* \leq x^* \tag{A1.25}$$

$$= \rho_f \left(e^{\frac{-x^*}{Pe}} - e^{\frac{\ell^* - x^*}{Pe}} \right) \qquad \ell^* \leq x^* \tag{A1.26}$$

In charged region of the pore

Superposing (A1.23) and (A1.26):

$$\rho_m = \frac{\rho_f}{Pe^2} \left(-e^{Pe\,\ell^*} + e^{Pe\,x^*} \right) + \rho_f \left(e^{\frac{-x^*}{Pe}} - 1 \right) \qquad 0 < x^* < \ell^* \tag{A1.27}$$

$$\approx \rho_f \left(e^{-x^*/Pe} - 1 \right) \qquad 0 < x^* < \ell^* \tag{A1.28}$$

Appendix 2

Charge distribution across a diameter of a cylindrical pore

When an electrolyte is situated adjacent to a solid surface which acquires a net fixed charge by ion adsorption from the fluid, the remaining ions in the fluid will be redistributed in the electrolyte. The electric potential in the fluid will reach a maximum at points nearest to the solid surface and will tend to decay to zero at points distant from the surface.

For a long cylindrical pore of length ℓ and radius a containing an electrolyte at steady state, the Poisson-Boltzmann equation relating dimensionless potential ϕ^* to radial position in the pore is obtained in dimensionless form[13] as:

$$\frac{\lambda_D^{*2}}{r^*} \frac{\partial}{\partial r^*} \left(r^* \frac{\partial \phi^*}{\partial r^*}\right) = \sinh \phi^* \qquad \text{(A2.1)}$$

$$\lambda_D \equiv \left(\frac{\varepsilon_r \varepsilon_o D}{\sigma_o}\right)^{1/2} \qquad \text{(A2.2)}$$

The dimensionless variables are defined as: $r^* = r/a$, $\lambda_D^* = \lambda_D/a$ and $\phi^* = zF\phi/RT$. Here ε_r is the relative permittivity of the fluid, ε_o the permittivity of free space, D the ion diffusion coefficient and λ_D is the fluid Debye length based on external conductivity σ_o . Fig. (15) shows numerical solutions[14] of Eq. (A2.1) for varying Debye ratios and a fixed wall potential.

The mobile charge density ρ_m in a binary electrolyte at points within the pore is related to the dimensionless potential by:

$$\rho_m = -2zF\, C_o \sinh \phi^* \tag{A2.3}$$

where c_o is the cation or anion concentration in the neutral fluid, z the charge number and F is Faraday's constant. From Eq. (A2.3), curves corresponding to those of Fig. (15) showing the mobile charge density as a function of radial position in the pore may be obtained.

If the Poisson-Boltzmann equation is linearized by assuming low charge densities in a binary electrolyte the equation for the mobile charge density within the pore is found to be[12]:

$$\frac{1}{r^*} \frac{\partial}{\partial r^*} \left(r^* \frac{\partial \rho_m}{\partial r^*} \right) - \frac{\rho_m}{\lambda_D^{*2}} = 0 \tag{A2.4}$$

Eq. (A2.4) can be solved to give the mobile charge density in terms of radial position and the mean mobile charge density $\bar{\rho}_m$:

$$\frac{\rho_m}{\bar{\rho}_m} = \frac{1}{2\lambda_D^*} \frac{I_o(r^*/\lambda_D^*)}{I_1(1/\lambda_D^*)} \tag{A2.5}$$

where I_o and I_1 are modified Bessel functions of the first kind of order zero and one respectively. This solution is shown in Fig. (2) for a range of Debye ratios.

Both Fig. (2) and Fig. (15) show that for large Debye ratios, ion concentrations and potentials become uniform across the pore. For more complex pore cross-sectional geometries and for high fixed charges this

result will still apply provided Debye ratios are sufficiently large. Effective Debye ratios will, however, tend to decrease as fixed charge densities or wall potentials increase, due to the greater ion concentration within the pores. Jacazio et al[14] estimated from numerical solutions of Eq. (A2.1) that the effective sheath thickness δ_D inside a pore decreased with wall potential ϕ_w^* according to the relation

$$\frac{\delta_D}{a} \sim 1 - \exp\left(-\frac{\alpha\lambda_{D\ \text{outside filter}}^*}{\phi_w^*}\right) \tag{A2.6}$$

where α is a constant. Thus, as wall potentials increase effective Debye ratios within the filter must decrease.

A qualitatively similar result in terms of wall charges is obtained by an order of magnitude analysis of Poisson's equation in the radial direction in a cylindrical pore:

$$\frac{1}{r}\frac{\partial}{\partial r}\left(r\frac{\partial\phi}{\partial r}\right) = \frac{-\rho_m}{\varepsilon_r\varepsilon_o} \tag{A2.7}$$

Quasi-neutrality within the pore requires that the mobile charge be equal in magnitude to the fixed charge on the wall:

$$\rho_m = -\rho_f \tag{A2.8}$$

If the fixed cation and anion concentration on the pore wall are c_{+f} and c_{-f} respectively, then:

$$\rho_f = zF\,(c_{+f} - c_{-f}) \tag{A2.9}$$

When there is a high fixed negative charge on the pore walls ($c_{-f} >> c_{+f}$), the fixed charge is approximately given by $\rho_f \approx -zF\, c_{-f}$. Substituting into Eq. (A2.7):

$$\frac{1}{r^*}\frac{\partial}{\partial r^*}\left(r^* \frac{\partial \phi^*}{\partial r^*}\right) \approx -\frac{z^2F^2c_{-f}}{\left(\frac{\epsilon_r \epsilon_o RT}{a^2}\right)} \tag{A2.10}$$

If the change in dimensionless potential from the edge of the pore to the pore axis is $\Delta\phi^*$,

$$\Delta\phi^* \sim \frac{a^2}{\left(\frac{\epsilon_r \epsilon_o RT}{z^2F^2c_{-f}}\right)} \tag{A2.11}$$

or, in terms of the Debye length based on external conductivity:

$$\Delta\phi^* \sim \frac{a^2}{\lambda^2_{D\ \text{outside filter}}} \times \frac{c_{+f}}{2c_o} \tag{A2.12}$$

$$\sim \frac{\rho^*}{\lambda^{*2}_{D\ \text{outside filter}}} \tag{A2.13}$$

Here ρ^* is the charge ratio - the fixed charge in the pore wall divided by the absolute charge of the bulk, neutral fluid (Eq. (24)) which is computed by assuming all ions to be of the same size. Eq. (A2.13) indicates that:

$$\frac{\lambda^*_{D\ \text{inside filter}}}{\lambda^*_{D\ \text{outside filter}}} \sim \frac{1}{\sqrt{\rho^*}} \tag{A2.14}$$

which suggests the same qualitative behavior as Eq. (A2.6) - effective Debye ratios within the pore decrease as wall charge increases.

Appendix 3

The capillary model

The architecture of a real membrane or porous bed is complex, the flow taking place via the random interstices in a fibrous or granular structure. A filter may be characterized by a thickness h, a bulk permeability k and a porosity ε - the ratio of void volume of the filter to total volume. Additional data on the mean pore diameter and pore size distributions is sometimes available, being obtained by electron microscopy[15], mercury intrusion methods[16] or by bubble point measurements[17]. It is possible, however, to make a rational definition of an effective pore radius a and pore length ℓ in terms of the bulk filter properties and one additional physical constant. Hence the mean flow speed within a porous bed may be evaluated from the superficial flow rate.

The permeability coefficient k is defined in terms of Darcy's law:

$$\frac{Q}{A} = -\frac{k}{\mu}\frac{\Delta p}{h} \qquad \text{(A3.1)}$$

Here Q is the superficial volume flow rate, A the cross-sectional area of the bed, Δp the pressure drop across the bed, h the bed thickness and μ the viscosity of the permeating fluid. If a filter is assumed to be traversed by a total of n tortuous channels of constant radius a and effective length ℓ, through which the fluid flows by Poiseuille flow, the permeability of the bed is given by:

$$k = \frac{n\pi a^4}{8A}\,\frac{h}{\ell} = \frac{n\pi a^4}{8aT} \qquad \text{(A3.2)}$$

We define the quantity ℓ/h to be the tortuosity T of the filter. It is the ratio of the distance travelled by some statistically "typical" fluid particle in moving through the filter to the thickenss of the filter. This definition of tortuosity differs from that adopted by some investigators who define tortuosity as the ratio of the permeability of an otherwise equivalent filter traversed by straight cylindrical pores to the actual permeability of the filter. In our capillary model this ratio will be shown to be the tortuosity squared.

The filter porosity and the specific filter surface exposed to the fluid S_o (surface exposed to the fluid per unit volume of solid) are given by:

$$\epsilon = \frac{n\pi a^2 \ell}{Ah} = \frac{n\pi a^2 T}{A} \qquad \text{(A3.3)}$$

$$S_o = \frac{n2\pi a\ell}{(1-\epsilon)Ah} = \frac{2\pi naT}{(1-\epsilon)A} \qquad \text{(A3.4)}$$

Eliminating n and a from Eq. (A3.2) - Eq. (A3.4) the expression for permeability becomes:

$$k = \frac{\epsilon^3}{2T^2 S_o^2 (1-\epsilon)^2} \qquad \text{(A3.5)}$$

This can be compared with the Kozeny-Carman relation - an empirical correlation - which gives the permeability as[17]:

$$k = \frac{K \varepsilon^3}{S_o^2 (1-\varepsilon)^2} \tag{A3.6}$$

where K is the Kozeny constant. Carman[11] showed that with $K = 1/5$ Eq. (A3.6) applies to a wide class of porous materials. The capillary model is clearly consistent with the Kozeny-Carman relation when the filter tortuosity is related to the Kozeny constant by:

$$T = 1/\sqrt{2K} \tag{A3.7}$$

This indicates that tortuosities are typically about 1.6.

The capillary model gives the effective pore radius in terms of bulk properties as:

$$a = 2\left(\frac{k}{\varepsilon K}\right)^{1/2} \tag{A3.8}$$

and the mean flow speed within a pore in the bed is found to be:

$$V = \frac{QT}{\varepsilon A} \tag{A3.9}$$

Appendix 4

Effect of charge cloud on local conductivity

When an electrolyte contains a net charge existing as a charge cloud in the fluid, the electrolyte conductivity will differ from that of the neutral fluid. For a weak electrolyte this change in conductivity can be expressed as a function of the local charge density only, provided the fluid is taken to be at equilibrium. Vellenga and Klinkenberg[18] have obtained general results for charge relaxation and the associated conductivity changes. Here we present only a simple derivation which assumes the electrolyte is at equilibrium.

We may represent an electrolyte by:

$$\underset{\text{electrolyte}}{\text{undissociated}} \rightleftharpoons A^+ + B^- \qquad \text{(A4.1)}$$

At equilibrium the product of cation and anion concentrations c_+ and c_- must be a function of the concentration of undissociated electrolyte c_u :

$$c_+c_- = f(c_u) \qquad \text{(A4.2)}$$

For a weak electrolyte $c_u >> c_+ , c_-$ and thus changes in ionic concentrations will not significantly change the concentration of undissociated electrolyte. The product c_+c_- will therefore remain essentially invariant. If in the neutral fluid cation and anion concentrations have equal values c_o , then generally:

$$c_+c_- = c_o^2 \qquad \text{(A4.3)}$$

For low Peclet number filtration of weak or strong electrolytes Eq. (A4.3) is consistent with Donnon equilibrium across the inlet of the filter. For a weak electrolyte flowing through a filter bearing a uniform fixed charge Eq. (A4.3) will also hold at all points in the void regions of the filter and outside the filter provided temperatures are uniform and the electrolyte remains at equilibrium. Inside the filter, quasi-neutrality, Eq. (2), requires that the magnitude of the charge density in the fluid $\bar{\rho}_m$ equal that of the fixed charged density of the filter:

$$|\bar{\rho}_m| = |\bar{\rho}_f| \tag{A4.4}$$

while outside the filter the charge density in the fluid is zero for low Peclet number flows.

For a binary electorlyte in which both ion types have equal diffusion coefficients D the fluid conductivity at any point is given by:

$$\sigma_m = \frac{z^2F^2D(c_+ + c_-)}{RT} \tag{A4.5}$$

while the neutral fluid conductivity is:

$$\sigma_o = \frac{2z^2F^2Dc_o}{RT} \tag{A4.6}$$

The absolute charge density ρ_o in the neutral fluid is defined to be the total charge in the fluid when all ions are taken to have a positive charge:

$$\rho_o = 2c_o zF = \frac{\sigma_o RT}{zFD} \tag{A4.7}$$

The mobile charge density is given by:

$$\rho_m = zF(c_+ - c_-) \tag{A4.8}$$

We define the charge ratio as:

$$\rho^* = \left| \frac{\rho_m}{\rho_o} \right| \tag{A4.9}$$

Combining Eq. (A4.3), (A4.7), (A4.8):

$$c_+ = \frac{\rho_m + \sqrt{\rho_m^2 + \rho_o^2}}{2zF} \tag{A4.10}$$

$$c_- = \frac{2c_o^2\, zF}{\rho_m + \sqrt{\rho_m^2 + \rho_o^2}} \tag{A4.11}$$

Eq. (A4.10) and Eq. (A4.11) can be summed to give:

$$\frac{c_+ + c_-}{2c_o} = \frac{\sigma_m}{\sigma_o} = \rho^* + \frac{1}{\rho^* + \sqrt{\rho^{*2} + 1}} \tag{A4.12}$$

$$\frac{\sigma_m}{\sigma_o} \approx 1 \quad \text{when} \quad \rho^* << 1 \tag{A4.13}$$

$$\frac{\sigma_m}{\sigma_o} \approx \rho^* \quad \text{when} \quad \rho^* >> 1 \tag{A4.14}$$

For the flow conditions considered in our theoretical solutions for filtration:

$$\rho^* = \left| \frac{\bar{\rho}_m}{\bar{\rho}_o} \right| \qquad \text{(A4.15)}$$

$$= \left| \frac{\bar{\rho}_f}{\rho_o} \right| \qquad \text{inside filter, Pe << 1} \qquad \text{(A4.16)}$$

$$= 0 \qquad \text{outside filter, Pe << 1} \qquad \text{(A4.17)}$$

Appendix 5

The hydrocarbon fluid

n-Heptane (c_7H_{16}) was selected as an appropriate hydrocarbon liquid to use in the charging experiments. It is a simple, readily available aliphatic hydrocarbon and its behavior is expected to be typical of most alkane and alkene hydrocarbon liquids. Aircraft fuels are largely aliphatic in composition and the filtering of these fuels presents one of the important charging problems commonly encountered[19]. The physical properties of heptane of possible importance in charging phenomena are fairly representative of many hydrocarbon liquids as shown in Table 3. The heptane molecule is highly non-polar and in this respect is also typical of the majority of hydrocarbon liquids.

The heptane used was obtained in a "pure" grade and is quoted by the manufacturer as 99 mole% pure. The heptane as received had a conductivity of about $1.6 \times 10^{-12}\ \Omega^{-1}\ cm^{-1}$, compared with the conductivity of chemically pure heptane which is less than $1 \times 10^{-13}\ \Omega^{-1}\ cm^{-1}$*. The conductivity of the heptane was increased by a factor of about four or more by the addition of the ionizing additive, ASA #3, in all experiments. This ensured that the electrokinetic effects involved primarily the known, controlled contaminant.

---

* Source: International Critical Tables.

Appendix 6

The Ionizing Additive

Changes in the conductivity of the heptane were brought about by the addition of minute amounts of Shell Antistatic Additive No. 3 (ASA #3)[20] kindly provided by Shell Chemical Company. The additive is manufactured expressly for the purpose of increasing conductivity in fuels[19] to reduce electrostatic hazards in fuel handling operations. ASA #3 is a mixture of equal parts of chromium dialkylsalicylate, calcium didecyl sulfosuccinate, copolymer of lauryl methacrylate and methylvinlpyridine as s 50% solution in a hydrocarbon solvent[21]. It has a specific gravity is about .93 at $20^{o}C$.

It is unfortunate that no information could be obtained on the diffusion coefficients of the dissociated ASA #3 ions. Values of these diffusion coefficients are essential for the complete analysis of the experimental data that has been obtained. However a wide variety of molecular diffusion coefficients in hydrocarbon liquids such as methanol, ethanol and benzene are available, and these are all close to 1×10^{-5} cm^2/sec *. In the absence of more definitive information it seems reasonable to assume that the ASA#3 ions have diffusion coefficients close to this value.

Because of the extremely low concentrations of additive required to obtain the desired conductivities a stock solution of 1000 parts per

---

* Source: International Critical Tables

million (ppm) by volume of the additive in heptane was prepared, and this was then added in small quantities to pure heptane. Fig. (16) shows the variation in the conductivity of heptane with concentration of ASA #3 added. It is interesting that the variation is approximately linear. For a weak binary electrolyte the conductivity varies as the square root of the nominal electrolyte concentration. It has been suggested[22],[23] that the linear dependence for ASA #3 results from bimolecular dissociation represented by:

$$A_m B_m + A_n B_n \rightleftharpoons (A_{n+1} B_m)^+ + (A_{n-1} B_n)^- \qquad \text{(A6.1)}$$

The reaction partners of:

$$AB \rightleftharpoons A^+ + B^- \qquad \text{(A6.2)}$$

would be virtually absent. This behavior is qualitatively explained if the binding energies of the particles in the reaction of Eq. (A6.1) are coulombic in nature. In this case the heat of the bimolecular dissociation is lower than that of the monomolecular reaction shown in Eq. (A6.2). We note here that Eq.(A4.12)-Eq. (A4.14) derived in Appendix 4 for a weak electrolyte are unchanged if bimolecular dissociation occurs, as long as the electrolyte is still "weak" - that is, the concentration of undissociated electrolyte must always greatly exceed ion concentrations in the electrolyte.

The temperature dependence of conductivity was not specifically investigated. Conductivity measurements were made, however, immediately after experimental data was taken, and this allowed for both temperature associated changes and for possible changes in conductivity resulting from the removal of colloidal particles by filtration or sedimentation.

Maximum recorded variations in measured conductivity at any given concentration of ASA #3 were no more than about 20%. Klinkenberg[22] mentions that the temperature coefficient of conductivity for ASA #3 in kerosene is close to that of the viscosity coefficient and attributes this to the same factors which bring about bimolecular dissociation, as already discussed. The influence of temperature on the equilibrium constant is suggested to be not more than about 10% of the temperature coefficient of conductivity.

Appendix 7

Measurement of Conductivity

The conductivities of hydrocarbon liquids are not as easily measured as those of aqueous solutions. A variety of experimental difficulties may be encountered in the determination of conductivities below about $10^{-10}\ \Omega^{-1}\ cm^{-1}$. These difficulties are briefly discussed here and the two experimental approaches commonly adopted to determine these low conductivities are outlined. The method chosen in this investigation is presented in detail.

Experimental Difficulties

1) Polarization The passage of a direct current through an electrolyte may cause chemical changes in the vicinity of the electrodes which act counter to the passage of the current. Factors which may contribute to polarization are electrolyte concentration changes in the fluid near the electrodes, the accumulation of products of electrolysis on the electrodes and the normal electrochemical electrode potentials.

For determining the conductivities of aqueous solutions the problem of polarization is often overcome by the use of alternating currents. This is only possible, however, when the relaxation time of the fluid is short in comparison with the cycle time of the applied A.C. For a hydrocarbon fluid of conductivity $10^{-12}\ \Omega^{-1}\ cm^{-1}$ the relaxation time is of the order of .2 seconds and thus direct currents must be used.

Polarization will generally be manifested as a decay of the current passed with time, from a maximum value occurring immediately after the potential is applied. For this reason the initial current recorded is used

in preference to the steady state current for the determination of conductivity. To overcome the problem of polarization potentials very high applied voltages are sometimes used. Above a certain field strength, however, Ohm's law is no longer obeyed[24],[25].

2) Electrolyte Adsorption The adsorption of the electrolyte to the electrode surfaces has been cited as a problem in measuring conductivities at low electrolyte concentrations[26].

3) Changes in Conductivity With Time The conductivity of many solutions in hydrocarbons is often found to decrease with time. This has been attributed to the colloidal characters of these solutions which may cause the establishment of internal equilibrium to proceed very slowly[1].

4) Electrolysis When D.C. methods are used to measure conductivity the number of ions removed may be a substantial fraction of the number originally present. If the electrolyte fails to regenerate ions as fast as they are removed the conductivity will decrease with time as the measurement proceeds. Correct values of conductivity are again obtained by extrapolation of measured currents to zero time[27],[28]. The dependence of conductivity on time during a D.C. measurement may be related to the rates of dissociation and association of the electrolyte[29].

Procedures for measuring conductivity

Two methods are commonly used for measuring electric conductivities of petroleum products. The first involves measuring the decay time of a standard condenser in which the solution under investigation acts as the dielectric through which charge leakage occurs. The second consists of a more direct determination by applying a steady potential across two surfaces separated by the liquid and measuring the current passed. Both

approaches are fully described by Klinkenberg[1]. A variation of the latter type of experiment was used in this investigation.

Apparatus

A 93 volt battery was used to drive current through a conductivity cell containing 1000 cm^3 of the solution under investigation. The conductivity cell consisted of two concentric stainless steel cylinders, similar to the cell used by Gavis and Wagner[3]. A Keithley 610B multistage electrometer was used to measure currents and the output from the electrometer was recorded on a Hewlett Packard 135 X-Y recorder.

Experimental Procedure

To determine a conductivuty, 1000 cm^3 of the liquid to be tested was placed in the cell which had previously been cleaned and rinsed with the same liquid. All parts of the cell were earthed for at least one hour to assure the complete relaxation of any charge generated in pouring or residual from the charging experiments. The power source and electrometer were then connected and the cell current was recorded from the electrometer output as a function of time.

In all determinations the current recorded tended to decay from an initial peak value. It was found that while peak currents obtained for different applied voltages were consistent with each other the rate of decay and final steady state currents were not consistent for these different driving potentials. This observation suggested that concentration polarization or electrolysis was occurring. The current recorded at effectively zero time was therefore used for all calculations of fluid conductivity.

Appendix 8

The Millipore filters[30]

Millipore filters of the MF type were used in all charging experiments. Two pore sizes were used. These filters consist of mixed cellulose esters and are relatively inert to most organic solvents. They are available in controlled thickensses with specified mean pore diameters. Variations in filter thicknesses and pore diameters are quoted as less than about $\pm$ 10% from the mean values. The characteristics of the filter types used are shown in Table 4.

The solid constituent of the filters was estimated to have a conductivity less than $10^{-13}\ \Omega^{-1}\ cm^{-1}$ by direct measurements on a dry filter.

Appendix 9

Transient charging phenomena

Transient currents were observed when a fresh filter was mounted in the charging apparatus and tested immediately. Generally the sign of the initial streaming currents was opposite to that of the steady streaming currents. For a constant flow rate through a fresh filter streaming currents usually increased from zero to an intermediate, steady, negative value, then decayed back to zero and eventually increased to a final steady positive value. The time scales involved were usually of the order of several hours, but sometimes considerably longer. If a filter was allowed to dry after being tested and then replaced in the test cell similar transients were again observed.

A more detailed and quantitative examination of these transient phenomena may help to explain the exact nature of the fixed charge acquired within the filter, the mechanism by which this charge is established and possible ways of reducing or otherwise affecting the development of such charge. Several experiments on transient charging phenomena of this kind have been conducted by other investigators[5],[6].

Appendix 10

Comparison with hyperfiltration theory

An analysis based on a model similar to the one employed in this study has been performed for salt rejection in hyperfiltration through porous materials[14]. In this analysis by Jacazio et al the dimensionless wall potential ϕ_w^* within the porous material is taken to be constant, in contrast to the constant wall charge model that has been adopted here. The two treatments do however yield similar results in the limit of high wall charge, convection-dominated flow conditions. An equation for the zero-current streaming potential for large Debye ratio flows is obtained by Jacazio et al as:

$$\frac{zF}{RT}\Delta\phi = -\tanh\phi_w^* \ln\left[(1-\cosh\phi_w^*) + e^{\frac{Pe\,\ell}{\lambda_D}}\cosh\phi_w^*\right] \qquad \text{(A10.1)}$$

When $Pe\,\ell/\lambda_D \gg \phi_w^* \gg 1$, (Eq. A10.1) reduces to:

$$\frac{zF}{RT}\Delta\phi = -\frac{Pe\,\ell}{\lambda_D} = -\frac{V\ell}{D} \qquad \text{(A10.2)}$$

which is a special form of Eq. (27) derived in our analysis for high charge ratio flows.

Appendix 11

Flux equations in coupled form.

Previous investigators have analyzed charging problems for flows through membranes using irreversible thermodynamics[7]. We note here that our model is entirely consistent with the results of these other investigations, and indeed may be used to obtain explicit expressions for the Onsager coefficients in terms of physical properties of the membranes. A general derivation of the Onsager coefficients for a capillary model is presented by Gross and Osterle[13]. The modifications that must be made to our model to obtain equations in coupled form as derived using irreversible thermodynamics are summarized here.

Two effects were neglected in our model since they are rarely significant in flows of weak electrolytes: coupling between fluid flow rate and electrostatic body forces, and the additional driving force that exists when the electrolyte concentrations upstream and downstream of a filter are different. Both of these effects are easily included in our analysis and the following flux equations are obtained[31] for high wall charge high Debye ratio flows:

$$j_{fluid} = L_{11}\,\Delta P + L_{12}\,\Delta\left(\phi + \frac{RT}{F}\,\ell n\ c\right) \qquad \text{(A11.1)}$$

$$j = L_{21}\,\Delta P + L_{22}\,\Delta\left(\phi + \frac{RT}{F}\,\ell n\ c\right) \qquad \text{(A11.2)}$$

$$L_{11} = \frac{\pi a^2}{8\mu\ell} \tag{A11.3}$$

$$L_{12} = L_{21} = \frac{\pi a^2}{8\mu\ell} \bar{\rho}_f \tag{A11.4}$$

$$L_{22} = \frac{D\bar{\rho}_f}{\ell RT} \left(1 + \frac{\pi a^2}{8\mu} \frac{\bar{\rho}_f RT}{FD} \right) \tag{A11.5}$$

Here j_{fluid} is the fluid flux rate, j is the current flux, ΔP the pressure difference across the filter and $\Delta(\phi + \frac{RT}{XF} \ln c)$ is the total potential difference (electric and electrochemical) between the upstream and downstream sides of the filter where c is the electrolyte concentration. Ion charge numbers have been taken to be unity.

REFERENCES

1. A. Klinkenberg and J. L. van der Minne, Electrostatics in the Petroleum Industry, (Elsevier Publishing Co., Amsterdam, 1958).

2. D. J. Shaw, Introduction to Colloid and Surface Chemistry (Butterworths, London, 1970).

3. J. Gavis and J. P. Wagner, "Electric Charge Generation During Flow of Hydrocarbons Through Microporous Media", Chem. Eng. Sci., 23, 381 (1968).

4. J. T. Leonard and H. W. Carhart, "Effect of Conductivity on Charge Generation in Hydrocarbon Fuels Flowing Through Fiber Glass Filters", J. Colloid and Interface Sci., 32, 383 (1969).

5. J. L. Lauer and P. G. Antal, "Electrostatic Charge Generation During Nonuniform Flow of Hydrocarbons Through Porous Insulators", J. Colloid Interface Sci., 32, 407 (1969).

6. J. L. Lauer and P. A. Antal, "How Electrostatic Charges are Generated by the Flow of Organic Fluids Through Filter Membranes and What Can be Done to Reduce Concomitant Safety Hazards", presented at the 64th Annual Meeting A.I.Ch.E., Hazards and Control of Static Electricity, San Francisco, (1971).

7. G. Tanny, E. Hoffer and O. Kedem, "Streaming Potentials During Hyperfiltration", Biological Aspects of Electrochemistry, Proceedings of the First International Symposium, Rome (Italy), (1971).

8. K. Sollner, I. Abrams and C. W. Carr, "The Structure of the Collodion Membrane and Its Electrical Behavior", J. Gen.Physiology, 24, 467 (1940).

9. A. Ilani, "Ion Discrimination by 'Millipore' Filters Saturated with Organic Solvents", Biochimica et Biophysica Acta, 94, 415 (1965).

10. P. Sennit and J. P. Olivier, "Colloidal Dispersions, Electrokinetic Effects and the Concept of Zeta Potential", Chemistry and Physics of Interfaces, Am. Chem. Soc., Washington.

11. P. C. Carman, Trans. Inst. Chem. Eng. Lond.,15, (1937); 16, 168 (1938); J. Soc. Chem. Ind., 57, 225 (1938).

12. J. Gavis and I. Koszman, "Development of Charge in Low Conductivity Liquids Flowing Past Surfaces: A Theory of the Phenomenon in Tubes", J. of Colloid Sci., 16, 375 (1961).

13. R. J. Gross and J. F. Osterle, "Membrane Transport Characteristics of Ultrafine Capillaries", J. Chem. Phys., 49, 228 (1968).

14. G. Jacazio, R. F. Probstein, A. A. Sonin and D. Yung, "Electrokinetic Salt Rejection in Hyperfiltration Through Porous Materials, Theory and Experiment" , J. Phys. Chem., 76, 4015 (1972).

15. F. M. O'Leary, G. E. Hess, F. E. Kulbaski and J. A. Shanahan, "Determination of Membrane Filter Pore Size by Electron Microscopy and Their Relationship to Colony Growth", Am. J. Bacteriol. Proc., A28, 31 (1965).

16. E. Honold and E. L. Skau, "Application of Mercury Intrusion Method for Determination of Pore-Size Distribution to Membrane Filters", Science, 120, 805 (1954).

17. A. E. Scheidegger, The Physics of Flow Through Porous Media, (Univ. of Toronto Press, Toronto, 1963).

18. S. J. Vellenga and A. Klinkenberg, "On the rate of discharge of electrically charged hydrocarbon liquids", Chem. Eng. Sci., 20, 923 (1965).

19. M. I. Yaffee, "Airlines Trying Anti-Static Fuel Additive", Aviation Week and Space Technology, p. 26, 30 Nov.,1964.

20. Shell Technical Bulletin ICSX: 69:5, "Shell Anti-Static Additive ASA-3", (Dix (Charlmont Press) Ltd., London).

21. Chemical Week, p. 45, 26 Dec., 1964.

22. A. Klinkenberg, "Static Electricity in Liquids", 1967 Static Electrification Conf., p. 63.

23. A. Gemant, Ions in Hydrocarbons, (New York: Interscience, 1962), pp. 48-49.

24. D. W. Goodwin and K. A. MacFadyen, "Electrical Conduction and Breakdown in Liquid Dielectrics", The Proceedings of the Physical Society (London), Section B, Vol. 66, No. 2, pp. 85-96 (1953).

25. H. House, "Dielectric Strength of Organic Liquids", Nature, 176, 610 (Sept. 24, 1955).

26. N. L. Cox, C. A. Kraus and R. M. Fuoss, "Properties of Electrolytic Solutions. XVI Conductance of Electrolytes in Anisole, Ethylene Bromide and Ethylene Chloride at 25°", Trans. of the Faraday Society, 31, Part 4, 749 (1935), 32, Part 4, 594(1936).

27. A. Klinkenberg, "Electrical Conductivity of Low Dielectric Constant Liquids by D. C. Measurement", J. Inst. Petrol., 53, 57 (1967).

28. C. Douwes and M. Van der Waarden, "Current Decay During Measurement of dc Electric Conductivity in Solutions in Hydrocarbons", J. Inst. Petrol., 53, 237 (1967).

29. M. Silver, "Conduction of Electricity in Insulating Liquids", J. Chem. Phys.,42, 1011 (1965).

30. Millipore Catalcgue MCl, Aug., 1972, Millipore Corp. (1970).

31. A. A. Sonin, private communication, April, 1973.